Vidhiaza Leviandhika

TRIBOLOGICAL PERFORMANCE OF C-ALLOYED WS_2 COATINGS WITH GRADED AND CONVENTIONAL STRUCTURES

VOLUME 1

Dissertação no âmbito do Mestrado Conjunto Europeu em tribologia de Superfícies e interfaces orientada pelo Doutor Todor Vuchkov e o Professor Albano Cavaleiro e apresentada ao Departamento de Engenharia Mecânica da Faculdade de Ciências e Tecnologia da Universidade de Coimbra.

Julho de 2021

TRIBOLOGICAL PERFORMANCE OF C-ALLOYED WS_2 COATINGS WITH GRADED AND CONVENTIONAL STRUCTURES

Submitted in Partial Fulfilment of the Requirements for the Degree of European Joint European Master in Tribology of Surfaces and Interfaces.

DESEMPENHO TRIBOLÓGICO DE REVESTIMENTOS DE WS_2 LIGADOS COM C COM ESTRUTURAS CONVENCIONAL E EM GRADIENTE

Author

Vidhiaza Leviandhika

Advisors

Albano Cavaleiro

Todor Vuchkov

Jury

President	**Professor Bruno Trindade** **Universidade D Coimbra**
Vowel	**Filipe Fernandes** **Universidade D Coimbra**
Advisor	**Doctor Todor Vuchkov** **Instituto Pedro Nunes**

---

1 2 9 0

UNIVERSIDADE D COIMBRA

tribos

Joint European Master in Tribology of Surfaces and Interfaces

Ljubljana • Leeds • Coimbra • Luleå

Coimbra, Julho de 2021

Acknowledgements

I would like to express my deepest appreciation to my supervisors Professor Albano Cavaleiro and Doctor Todor Vuchkov, without whom this thesis project would not come to fruition. Their guidance, patience, and ideas have helped me massively from the planning to the execution of this project. I could not have imagined having better supervisors and mentors for my master thesis project.

Besides my supervisors, I would like to thank the TRIBOS teaching staff in University of Leeds, University of Ljubljana, and University of Coimbra. The knowledge that they shared has been very valuable for this project and I have had a pleasant experience in the classes. I would like to especially thank the coordinators of TRIBOS in each university, namely, Professor Ardian Morina, Professor Mitjan Kalin, and Professor Bruno Trindade.

My sincere gratitude also goes to the staff of Instituto Pedro Nunes who contributed to the many experiments of this project, including the coating deposition and coating characterization.

Lastly, I would like to thank my TRIBOS classmates for their support and companionship for these past two years.

Abstract

The increasing restriction on the use of environmentally harmful materials pushes industrial needs to shift away from conventional lubricants. Thin film coatings based on transition metal dichalcogenides (TMDs) have shown promising attributes to be an effective solid lubricant. The inherent weakness of TMDs, their low hardness, can be improved by alloying them with carbon. The coating to be studied in this work is W-S-C, a TMD-based coating which is thought to perform best when it has ~50 at.% of carbon content.

The aim of the present study was to investigate the tribological performance of three types of W-S-C coatings, namely, a reference W-S-C coating with ~50 at.% carbon, a W-S-C with reduced carbon content at ~35 at.%, and a W-S-C coating with a graded structure. The coating with graded structure had carbon-rich W-S-C on the bottom layers with gradually reducing carbon content on the upper layers and finished with pure WS_2 on the top layer.

The tribological performance was tested by reciprocating ball-on-disk tribometer under ambient air at room temperature, under dry N_2 environment at room temperature and under elevated temperature of 200°C. It was found that each coating showed self-adaptive behavior under every operating condition, though for each condition, there was one coating that performed particularly well. The reduction of carbon content from ~50 at.% to ~35 at.% was coupled with the increase in WS_2 content. This in turn enhanced the coating's performance under dry N_2 and at 200°C significantly while still being effective under room temperature. The coating with graded structure also shows superior performance compared to the coating with ~50 at.% under dry N_2 and at 200°C. However, the coating could not reach a steady state COF and produced comparably higher wear under room temperature due to the frequent formation and removal of WS_2 tribolayer. This study showed the prospect of improving the tribological performance of W-S-C coatings in a variety of environments through the alteration of the composition and structure.

Keywords: Transition metal dichalcogenides, gradient structures, self-adaptive coatings, W-S-C coating, tribology.

Resumo

As restrições crescentes na utilização de materiais perniciosos para o meio ambiente tem obrigado as empresas a procurar soluções alternativas aos lubrificantes convencionais. Os revestimentos finos à base de dicalcogenetos de metais de transição (TMD) têm mostrado atributos que lhes permitem ser eficientes como lubrificantes sólidos. A maior desvantagem destes materiais, a sua baixa dureza, pode ser melhorada através da adição de carbono. O revestimento a ser estudado neste trabalho é um W-S-C, um revestimento à base de TMD, que tem um desempenho adequado quando o teor de C é de aproximadamente 50% at.

O objetivo deste estudo foi investigar o desempenho tribológico de três tipos diferentes de revestimentos W-S-C, nomeadamente, um W-S-C referência com 50 %at. de C, um W-S-C com teor de C mais reduzido (35 % at.) e um W-S-C com uma estrutura em gradiente. Nesta caso o revestimento tinha uma camada de W-S-C rica em carbono junto ao substrato, reduzindo o teor deste elemento à medida que se aproxima da superfície, terminando com uma camada no topo de WS_2 simples.

O comportamento tribológico foi avaliado num tribómetro, numa configuração tipo pino-disco, em atmosfera normal às temperatura ambiente e 200 ºC, assim como em azoto seco à temperatura ambiente. Todos os revestimentos mostraram um comportamento auto adaptável em todas as condições de teste tendo um em particular mostrado um excelente desempenho. A redução do teor de carbono de 50 para 35 %at. mostrou estar ligada com um aumento do teor de WS_2. Como resultado, o desempenho em azoto seco e a 200 ºC melhorou significativamente sendo também efetivo em ambiente normal. O revestimento com uma estrutura em gradiente também mostrou um desempenho melhor que o revestimento com 50 %at. de C quando testado quer em azoto seco quer a 200 ºC. Contudo, o revestimento não pôde alcançar um regime estável de COF e deu origem a um desgaste comparativamente maior em condições ambientais devido à sucessiva formação e destruição da tribocamada de WS_2. Este estudo mostrou a perspetiva de melhoria do desempenho tribológico de revestimentos de W-S-C em diversos ambientes de teste através da alteração da composição química e da estrutura.

Palavras-chave: Dicalcogenetos de metais de transição, estrutura em gradiente, revestimentos auto-adaptativos, W-S-C, tribologia.

Table of Contents

List of Figures

List of Tables

1. Introduction

Tribology is the science of interacting surfaces in relative motion. It is the study that tackles all problems related to friction, wear, and lubrication [1]. Though the name may not be familiar to the general public, tribology exists in virtually every part of modern society. Moving, sliding, and interacting parts are at the heart of transportation, power generation, and manufacturing. Knowledge of tribology is at play in ensuring these parts function their intended purpose with a certain degree of efficiency, reliability, safety, and durability. Hence, complications due to tribological contacts directly translate to expenditure, usually described as energy loss or energy consumptions. For this reason, tribology has a great economic influence.

An estimate from 2017 claims that tribological contacts took around 23% of global total energy consumption, which translates to 119 Exajoules [2]. Of this energy consumption, 103 Exajoules contributed to overcoming friction and 16 Exajoules went to wear-related maintenance and reparation. If the world is to take advantage of the best strategies for minimizing friction and wear problems, there potentially will be savings that worth 1.4% of the annual GDP and 8.7% of the total energy consumption [2]. A report of two years of investigation in the Chinese industry in 2006 echoes this result, stating that issues related to tribology are worth 1.55% of the country's GDP [3]. Though there has been fifty years break, these findings are consistent with The Jost Report that was published in 1966. The Jost Report, the first documentation that uses the word *tribology*, claimed that the cost of friction, wear, and corrosion to the UK economy amounted to 1.1 to 1.4% of GDP [4]. These findings point to the value of tribology very clearly, which is about 1.5% of GDP. Though the percentage value may be minute, it signifies massive energy and money savings, worth at least hundreds of millions of US dollars.

Aside from pure economics, engineers today face another pressing challenge, that is, the environmental impact of engineering systems. Oil-based liquid lubricants are classic tribological solutions. They are effective in reducing the friction of a mechanical system, protecting against wear, and regulating temperature. However, laws and regulations have become stricter with regards to the use of environmentally harmful products, which exist in many of the liquid lubricants [5]. As such, engineers today will have to consider equally important factors at the same time: to reduce losses and failures due to tribological contacts, and to minimize the system's impact on the environment. Fortunately, these two factors are not exactly conflicting. Certain solid lubricants show great tribological applications while having a low environmental impact. Solid lubricants come in the form of a coating on the surface.

They work by generating a tribofilm on the contact, offering low friction of the system and wear protection for the surfaces.

The solid lubricant of interest in this master thesis is carbon-alloyed WS_2 coating. WS_2 belongs to a class of material named transition metal dichalcogenides (TMD). Due to their structures, TMD materials – including WS_2 – have attractive properties for tribological applications. However, while a pure WS_2 thin film coating may be good to reduce friction in a system, its wear resistance is not up to par for tribological applications. Therefore, alloying WS_2 with inherently hard elements such as carbon will make a coating with adequate mechanical properties and good tribological properties.

The advantages of the incorporation of carbon to WS_2 coating are not limited to mechanical properties improvement. With carbon content, WS_2 coatings will also have an increased resistance to oxidation. Furthermore, carbon can assist to provide lubrication when moisture is present. However, the addition of carbon to WS_2 coatings are not without drawbacks since carbon may hinder the tribological performance of WS_2 under certain conditions. The amount of carbon must be carefully considered so that it will not eliminate the strength of WS_2, which is the formation of easily shearable layers. One potential way to produce a carbon-alloyed WS_2 coating that possesses the best of carbon and WS_2 properties is to fabricate a coating with a graded structure. This coating should have a carbon-rich layers at the bottom to produce layers with good mechanical properties. On the upper layers, the coating should have layers with reduced carbon coating so that the upper layers will stay easily shearable as significant amount of WS_2 resides there. The coating with this graded structure is the particular topic of interest of this study.

2. Framework

The research project titled “Tribological performance of C-alloyed WS_2 coatings with graded and conventional structures” was performed as a master thesis project as fulfillment of the requirement of Joint European Master’s Degree in Tribology of Surfaces and Interfaces. The project studied and compared the performance of various C-alloyed WS_2 coatings, namely, coatings with ~50 at.% C, coatings with ~35 at.% C, and coatings with graded structures. The work was performed at the University of Coimbra and Instituto Pedro Nunes.

3. State of the Art

This section is dedicated to reporting the current understanding of transition metal dichalcogenides, the centerpiece of the work presented in this thesis. As such, its structure and properties are discussed extensively. Relevant past and current researches are also examined to add further context.

3.1 Transition Metal Dichalcogenides

As the name suggests, transition metal dichalcogenides are a class of material composed of transition metal atoms (such as Mo and W), and dichalcogenide atoms (such as S, Se, and Te). Owing to its many attractive mechanical and electrical properties, TMDs are subject to researches in various applications, such as flexible electronics, energy harvesting, and medicine [6], [7]. Though TMDs finds use in numerous applications, its presence in tribology will be the focus of this section.

As a film coated on a substrate or as an oil additive, TMDs have found their place in friction-reducing applications [8]. The structure of TMDs can be credited for its ability to provide low-friction systems. However, TMDs have several weaknesses that prohibit it to thrive in the field, specifically its hardness and susceptibility to environmental attacks [8]. This is particularly a problem because a TMD film prepared by sputtering inherently possesses columnar structures with high porosity, which negatively affect its load-bearing capacity, oxidation resistance, and adhesion to the substrate [9], [10]. Over the years, studies have been performed to find solutions for these problems, including alloying the TMD material with harder materials and utilizing heat treatment after film deposition.

3.1.1 Structure

The transition metal dichalcogenides formula can be generalized as MX_2, with M and X representing the transition metal atom and chalcogenide atom, respectively. TMDs consist of alternating layers where 1 transition metal atom is sandwiched between 2 sets of chalcogenide atoms. Being highly planar, its crystal structure can be characterized as trigonal prismatic (2H, belonging to hexagonal crystal family) or octahedral arrangement (1T and 1T', belonging to tetragonal crystal family) [11]. In the trigonal prismatic structure, the atoms in the chalcogen layer are positioned directly opposite each other in a direction perpendicular to the layer. The chalcogen atoms on the same layer are also equidistant to each other. On the other hand, in the

1T arrangement, one chalcogen layer is shifted 180° from the opposite layer. From the 1T arrangement, the position of chalcogen atoms can be distorted further to create a 1T' arrangement. These TMD structures can also be described by their stacking order for ease of understanding. If we are to take the TMD atomic planes to be chalcogen – metal – chalcogen, then the stacking order of the trigonal prismatic structure is ABA [6]. ABA stacking order implies that the chalcogen atoms reside in the same position in their corresponding atomic plane. Conversely, 1T and 1T' structure possesses ABC stacking order, where the chalcogen atoms on the chalcogen planes reside in unique positions. Figure 1 depicts the common atomic structures of TMDs.

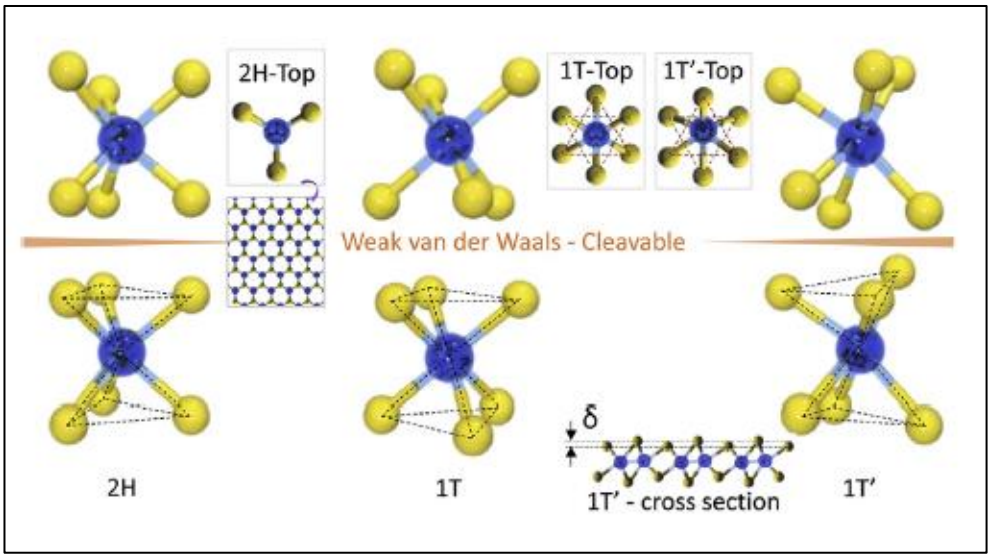

Figure 1. Atomic structure of a TMD layer in their trigonal prismatic (2H) and octahedral (1T and 1T') arrangement [11].

The hexagonal crystal structure, 2H, is especially important for tribological applications. This crystal structure ensures a sixfold symmetry, that is, the crystal appears the same when rotated by one-sixth turns. In hexagonal TMDs, each metal atom is surrounded by six equidistant dichalcogenide atoms, and each dichalcogenide atom is surrounded by three equidistant metal atoms. The hexagonal crystal structure also shows a laminar structure. These characteristics of the hexagonal crystal structure contributes to especially lubricous nature. It must be noted, however, even though the hexagonal TMDs is the most effective for tribological applications, other crystal structures can also be used for friction-reducing applications.

The bonding between the metal atom and the chalcogenide atoms is covalent. Contrasting this strong bonding, the TMD's lattice layers are bound by weak van der Waals bonding [12]. Consequently, the cohesive forces between the lamellae of TMDs will be easily sheared, even though TMDs can create strong adhesive force with a substrate. These characteristics, upon sliding and/or moving contact, will result in the preferential slip between lamellae as opposed to slip between individual lamella and the substrate if the adhesive forces between the TMDs and the substrate are stronger than its cohesive force between the lamellae. The interlayer shearing of its structure is the basis of the lubricating mechanism of TMDs. For this reason, the group of materials is attractive and practical for friction-reducing applications. One caveat of TMDs is that the thin film must be oriented in such a way that the basal planes (0002) are parallel to the sliding surface.

3.1.2 Properties

Perhaps the two most important basic properties for tribological coatings are hardness and adhesion as they are directly related to the expected endurance of the coating. Hardness directly relates to the longevity of the coating as it will minimize wear damage. Pure TMD materials usually have a hardness of about 0.3 to 2 GPa, though the exact value will vary depending on several factors such as the deposition technique employed, morphology and stoichiometry (X/M ratio) [8]. This value is nevertheless very poor for tribological applications. For context, another prevalent material for low-friction coatings, diamond-like-carbon has hardness up to 70 GPa [13]. However, alloying TMD with tougher materials such as titanium has been proven to improve the hardness by an order of magnitude.

Adhesion between the coating and the substrate must also be strong so that the coating will not delaminate upon sliding contact. TMD has generally low adhesion to the common substrates for tribological applications, such as steel [14]. Improvement to the adhesion between TMD coating and the substrate can be realized by adding an interlayer between them. Titanium and chromium have been used for the interlayer with relative success [14].

3.1.3 Presence in Tribology

TMDs have been studied extensively for its potential in tribological applications for decades. TMD materials have the potential to act as lubricant additives. Though conventional additive chemicals such as zinc dialkyldithophosphate (ZDDP) perform well as lubricant additives, TMD materials have an inherent advantage as a lubricant additive. TMD materials have better chemical stability and lower toxicity, making them a better alternative with regards to the

environmental impact. MoS_2 and WS_2 have been singled out for their effectiveness as lubricant additives [15]. In fact, another proven conventional lubricant additive, molybdenum dithiocarbamate (MoDTC), works by taking the advantages of a TMD material. The main mechanism of MoDTC for friction reduction is the in-situ formation of MoS_2 layers. This goes to prove that TMD materials can improve lubricants performance by further friction minimization.

TMD materials used as surface coatings fall on the solid lubrication category. To better capture how solid lubrication achieve friction reduction, an understanding of the mechanism of friction between two contacting metallic bodies should first be established. Though friction is generally looked as a surface phenomenon, the frictional force and the nature of sliding between metals are also directly related by the bulk properties of the metals, such as their hardness and melting points. The frictional force between contacting metals is mainly due to (1) shearing of the metallic junctions produced by adhesion and welding of the contacting bodies, and (2) dragging and ploughing of the softer metal's surface irregularities [16]. Solid lubricants reduce friction mainly by diminishing both the area over which metallic junctions form and break, and the strength of adhesion at these metallic junctions [16]. Accordingly, an effective solid lubricant should have a readily shearing layer (such as TMD materials) on top of a load-supporting layer with high hardness to isolate the metal surface underneath.

Advances in TMDs as tribological coating seem to be heading towards TMD nanocomposites. This is driven by the fact that pure TMD materials have a low load-bearing capacity, making them vulnerable to wear damage. Aside from mechanical properties, its susceptibility to oxidation may also hinder pure TMD materials to perform in tribological applications. It has been observed that TMD thin films oxidize in the air [13], [14]. This is because the edges of dichalcogenide atoms (such as sulfides and selenides) can react with surrounding molecules and form oxides [17]. Surface oxides have been reported to increase friction in the TMD system [18]. With all the intrinsic drawbacks of pure TMD materials, reinforcement of the TMD material with other materials must be done to realize their potential for tribological applications.

Research on TMDs as composite tribological coatings date back as early as the 1990s. In one such study, a TMD material was utilized as a coating for aerospace application [13]. In this study, WS_2 was embedded together with tungsten carbide inside an amorphous diamond-like carbon (DLC) matrix to form a nanocomposite structure [13], [19]. Upon space simulation

tests, the study reports a very low coefficient of friction (0.02 to 0.05) and endurance greater than two million cycles [13]. To achieve low coefficient of friction, the nanocomposite must have greater than ~20 at.% of sulfur. It is found that at these percentages, formation of crystalline WS_2 layer is initiated on the surface, which enables lubricity. With the same nanocomposite, Voevodin also introduced the concept of self-regulating 'chameleon' behavior of the coating [19]. Under humid air, WS_2 is protected from oxidation, leaving lubrication to DLC phase. In contrast, under dry nitrogen or vacuum environment, WS_2 crystallization occurs due to the friction, thus dominating the lubrication. This ability of self-regulation, which is depicted in figure 2, can be a very important concept to consider in the design of tribological coatings. These studies performed by Voevodin demonstrate a common theme with regards to advances in TMDs, which is combining a TMD material with tougher materials to form the product, creating a coating with superior lubrication and mechanical properties.

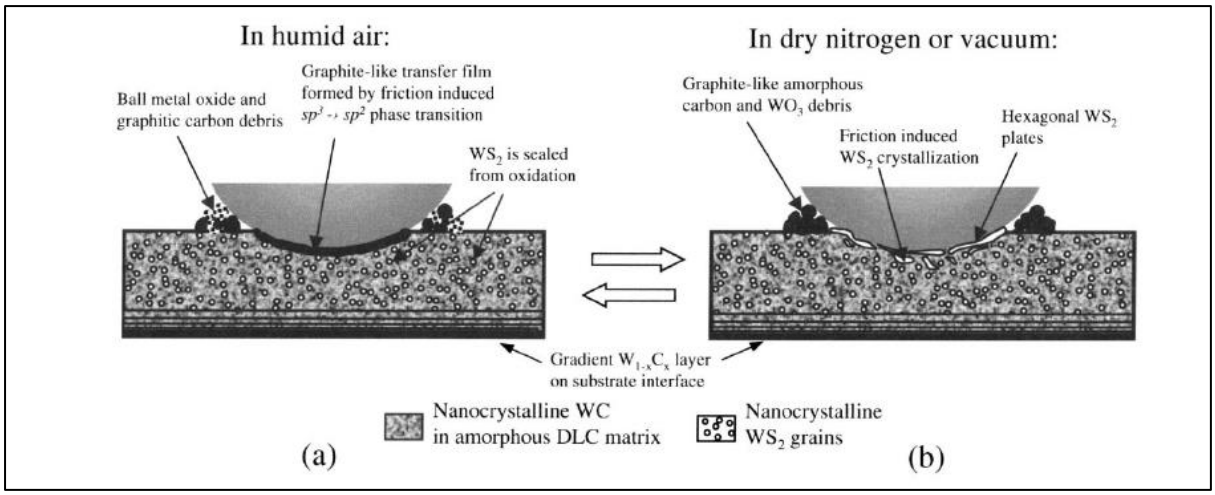

Figure 2. Self-adaptation mechanism of WC/DLC/WS_2 nanocomposite coatings to provide lubrication in humid air (a) and dry nitrogen or vacuum (b) environment [19].

In the same notion as the studies conducted by Voevodin, research on alloyed TMD have been performed using several different alloying materials. Carbon and nitrogen have been proven to be viable alloying elements for TMD. A study in 2011 conducted by Polcar and Cavaleiro successfully shows that carbon-alloyed WS_2, MoS_2, WSe_2, and $MoSe_2$ perform well even in humid air, owing to their self-adaptability (TMD thin film layer formation on contact and reorientation of TMD platelets in the matrix) characteristic [14]. The same study also shows the success of nitrogen alloyed WS_2 coatings in a moisture-free environment.

The previously mentioned studies are only two examples of many attempts in creating a TMD composite. Other than the studies, for instance, thin films of WS_2 have been doped with ZnO, and MoS_2 films have been doped with Ti, Al, and Ni. Though the alloying elements vary, the intention of alloying is the identical. Alloying is performed either to increase film density, strengthen the coating, and/or improvement in oxidation stability [20]. These factors will ultimately lead to coatings that are better suited for tribological applications.

3.1.4 Carbon-alloyed Transition Metal Dichalcogenides

It is well understood that TMD coatings provide low friction because they can form a tribolayer on contact. The tribolayer is composed of pure crystalline TMD material with its (002) plane oriented parallel to the sliding surface. This orientation is ideal to combat friction and oxidation [8], [21]. Typically, the formation of this low friction tribolayer marks the end of the running-in period of the system, after which the coefficient of friction finally reaches a steady state. However, with carbon-alloyed TMD coatings, the formation of tribolayer during the initial stages of sliding is not always guaranteed or adequate, prolonging the running-in period of the system. This is because with increasing carbon content, the coating may not have enough TMD material to support the formation of the tribolayer. As such, when incorporating carbon into a TMD-based coating, one must balance the chemical composition to optimize the friction-reducing capability without compensating the mechanical properties.

Over the past years, there have been research on the effect of chemical composition on the tribological performance of carbon-alloyed TMD coatings. Results from studies performed by Polcar and Cavaleiro in the 2000s suggested that the most optimal composition for W-S-C coating was ~50 at.% carbon and 27 at.% sulfur, with S/W ratio of around 1.2 and 1.3 [22], [23]. However, recent studies show that coatings with lower carbon content may also have promising properties [24]–[26]. Furthermore, these recent studies show that a greater S/W ratio is more advantageous than the low S/W ratio presented in Polcar's and Cavaleiro's studies.

A study conducted by Vuchkov et. al. in 2020 investigated the tribological performance of W-S-C coatings at ~50at% carbon with varying S/W ratio from 1.2 to 1.69 [24]. The study showed a contrasting performance of two coatings with similar sulfur content (at 27 at.% and 28 at.%) but different S/W ratios, one coating at 1.56 and the other at 1.4. The coating with S/W ratio of 1.4 experienced a total worn out during the tribotest, whereas the coating with higher S/W ratios achieved a steady-state COF at 0.1 – 0.15 during the test. In the study, the coating with the highest S/W ratio performed the best, having the shortest running-in period before it

reached a steady-state COF at 0.12 – 0.15. Raman analysis of the wear scars of the best performing coating showed sharp peaks belonging to crystalline WS_2. The author also noted that the coatings with low S/W ratios failed to form a tribolayer, contributing to their failures during the test. This study shows that the S/W ratio, along with the sulfur content, plays a crucial role in the formation of lubricous tribolayer of W-S-C coatings.

The findings from Vuchkov's study are echoed by another study conducted in 2019 by Cao et. al. Cao's study also showed that high values of S/W and sulfur content are desirable in the pursuit of improved performance for W-S-C coatings. Similar to the results reported by Vuchkov, Cao's study showed that the best performing W-S-C coatings had a high sulfur content at ~50 at.% and ~1.6 S/W ratio [25]. In Cao's study, intense WS_2 peaks in Raman analysis of the wear track of the best coating were also observed, indicating the abundant tribolayer formed on the surface. In this study, the best W-S-C coating only had ~20 at.% of carbon, signifying that coating with low carbon content can still perform well for tribological applications. This inference is shared by another study performed in 2020 by Yaqub et. al. In Yaqub's study, the performance of Mo-Se-C coatings with carbon content lower than 30 at.% was investigated. The results from this study indicated that the lower carbon content contributed to the ease of tribolayer formation, thus reducing the running-in period of the coating [26].

The results of past studies show the significance of composition to the performance of carbon-alloyed TMD coatings. Generally, a high X/M ratio is desired as it corresponds to better crystallinity of the TMD phase [26]. In addition, a higher TMD content (achieved by reducing the carbon content) is also favorable as it promotes the formation of tribolayer, effectively shortening the running-in period of the system. It must be noted however, a lower carbon content also corresponds to a coating with lower hardness.

3.2 Physical Vapor Deposition

Physical vapor deposition (PVD) defines a group of techniques that grows a thin film by atom deposition on a substrate. In physical vapor deposition, a condensed material called a "target" is forced to vaporize. The target's atoms in the vapor phase are then guided to a substrate material, on which they will condense and form a thin film. There two major processes that fall into the PVD category, namely sputtering and evaporation. In deposition via sputtering, energetic ions are accelerated to strike the target material, causing the material to be sputtered

and deposited to a substrate. On the other hand, evaporation deposition involves evaporating material in a vacuum and letting the evaporated atoms condense to a substrate.

For the purpose of this document, only magnetron sputtering deposition will be more extensively discussed as it is the process that is utilized for the TMD material growth in the work.

3.2.1 Sputter Deposition

The basic principle of sputter deposition is the ejection of atoms via energetic particles bombardment and letting the atoms condense onto a substrate. The particles involved in physical sputtering are usually ions from gaseous materials that are accelerated by an electric field [27]. Shown in figure 3 are several common configurations of sputtering, including magnetron diode, DC diode, RF diode, and ion beam sputtering.

The most basic configuration is DC diode sputtering system, with all other systems represent advancements from DC diode. DC diode sputtering system utilizes planar electrodes. The target material is placed on the cathode and the substrate is placed on a holder facing the cathode. Inside the chamber, Ar gas is maintained at a pressure of 1-5 Pa. Glow discharge is generated with DC power supply. The resulting Ar ions in the glow discharge are accelerated to the target material on the cathode causing sputtering of the atoms. Subsequently, the sputtered atoms will traverse the space between the cathode and the substrate and condense on the substrates. Due to the ionization of gas, DC diode sputtering system is only ideal for deposition of conductive materials. This is because the resulting positive ions will accumulate on the surface of the target.

The problem inherent in DC diode can be avoided by RF diode sputtering system, as it utilizes AC power supply instead of DC. In RF diode sputtering system, the positive ions will impinge on the surface during negative portion of the alternating potential, and they will be removed from the surface during the positive one. This ability enables RF diode sputtering system to deposit dielectric and poorly conductive materials.

The clearest difference between ion beam sputtering and other sputtering technique is that it allows direct control over the ions that will bombard the surface of the target. The technique relies on ion beam source to sputter the target. This gives the flexibility to control the ion beam energy, current, species, and angle of incidence. However, some disadvantages of the technique include a small area of bombardment and a low deposition rate. As such, ion beam sputtering is not ideal for large area deposition.

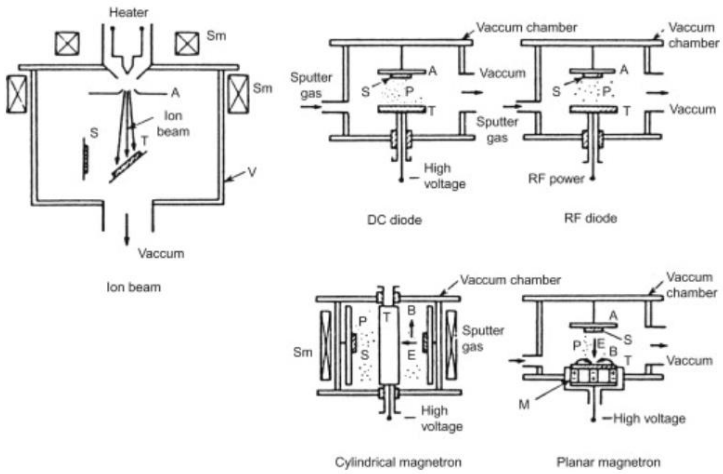

Figure 3. Common configurations of sputtering techniques [28].

3.2.2 Magnetron Sputtering

Compared to DC and RF diode sputtering systems, the magnetron sputtering system provides high purity film at a high deposition rate. This can be credited to the fact that magnetron sputtering is a low-pressure technique, reaching as low as 10^{-3} mbar inside the chamber (compared to 10^{-2} mbar of DC diode sputtering). In magnetron sputtering systems, magnets are placed on the cathode. The resulting magnetic field will entrap secondary electrons that are ejected during sputtering. The entrapped secondary electrons will then gyrate around the magnetic field and increase the probability of collision with the neutral argon gas. As such, a greater probability of ionization of the argon gas is achieved and thus a denser plasma will be generated. With higher-density plasma, an improved deposition rate is expected.

There are two types of magnetron sputtering, namely balanced/conventional magnetron and unbalanced magnetron. In a balanced magnetron sputtering system, one pole of the magnet is placed at the central axis of the target material and the other pole is placed on the edges. In this configuration, all magnetic field lines are closed between the central and the edge poles. On the contrary, in an unbalanced magnetron sputtering system, some magnetic field lines are directed towards the substrate by the strengthening or weakening of one of the poles [29]. Consequently, the electrons can follow the field lines and flow out of the confinement, increasing the ionization of the Ar gas in the proximity of the substrates. By application of a negative potential on the substrates, due to the increased ionization of the Ar gas in the proximity of the substrates, the substrates will be concurrently bombarded with Ar ions, which can be beneficial for the deposited films. Unbalanced magnetron can further be divided into

two types, namely, type 1 and type 2. In type 1 unbalanced magnetron, the central pole is the inception of all magnetic field lines. In type 2 unbalanced magnetron, some of the magnetic field lines do not touch the central pole as they originate from annular sources. In unbalanced magnetron sputtering, the magnets can be arranged in geometry to confine the plasma away from the wall chambers which will result in greater ion current density near the substrate. The technique with this type of magnet geometry is named closed-field unbalanced magnetron sputtering [30]. Figure 4 shows the arrangement of the different types of magnetron sputtering.

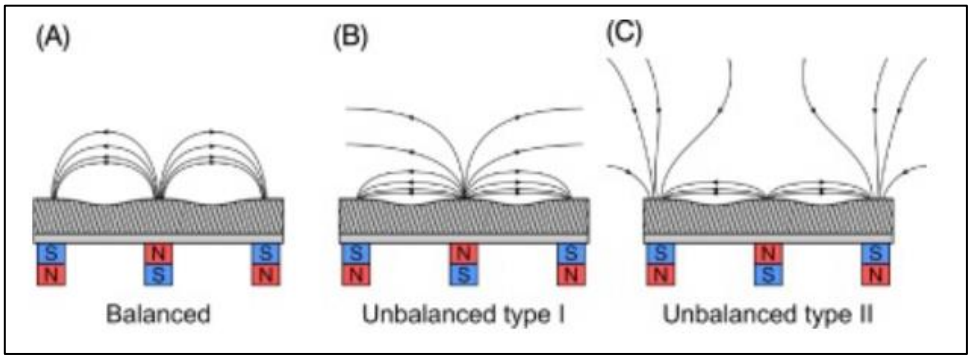

Figure 4. Schematic of balanced (A), type 1 unbalanced (B), and type 2 unbalanced (C) magnetron configurations [29].

Magnetron sputtering is a proven technique for the deposition of TMD films. Many studies of TMD in various fields prepared their samples via magnetron sputtering. For instance, McConney et. al. established a method for large-scale deposition of MoS_2 and WS_2 thin films (<10 nm) for semiconductor applications. The TMD films were deposited on PDMS and intended for the development of stretchable electronic nanodevice. In this study, magnetron sputtering was the chosen technique due to its viability for upscaling and its ability to deposit thin films free of defects and contamination [31].

Magnetron sputtering has also been utilized for deposition of TMD films intended for tribological applications. One study in 2011 employed magnetron sputtering with carbon target and WSe_2/MoS_2/WS_2 target simultaneously to deposit a carbon alloyed TMD thin film with great success [14]. More recently, a study performed a deposition of TMD thin film for tribological application at a larger scale using closed-field unbalanced magnetron sputtering. The study utilized a semi-industrial deposition unit to deposit $MoSe_2$ alloyed with carbon on Si wafers and steel cylinders [32].

The aforementioned studies are a few examples of many studies that show how magnetron sputtering technique can be applied for the deposition of various TMD films on various substrates. Magnetron sputtering simply has many advantages compared to other techniques that makes it ideal for TMD films deposition. The applications of TMD films usually require high purity, fast deposition, and large area coverage; All of which are within magnetron sputtering capabilities. As such, the technique will be employed for the film deposition of the work in this document.

4. Research Gaps

This thesis work is intended to study and compare the tribological performance of three different types of carbon-alloyed WS_2 coatings. One of these coatings will have carbon content of ~50 at.%, which will serve as a reference coating. One type of the coating will have reduced carbon content at ~35 at.%. The last coating will have a specially designed graded structure. The latter two coatings are designed with the expectation of an improved tribological performance from the reference coating in mind.

As discussed in the previous section, recent studies on C-alloyed TMD coatings showed that coatings with lower carbon contents of ~20-30 at.% of carbon can also provide good tribological performance. Due to the higher amount of TMD phase in the films, these coatings enable a faster formation of a lubricious tribofilm, resulting in shortened running-in periods and an improved coefficient of friction when compared to coatings with greater (e.g. ~50 at.%) carbon content. One potential drawback for coatings with lower carbon content can be a more porous morphology and reduced hardness, which can translate to lower wear resistance. A possible solution to improve the tribological performance of the coating without compensating its hardness is to deposit a film with a graded structure. The coating with graded structure will have layers of gradually decreasing carbon content, starting at the harder bottom layer with a high carbon content (~ 50% at. of carbon) and finishing with a pure WS_2 layer on top. This structure should provide softer top layers rich in WS_2 that will enable the fast formation of the lubricious tribolayers, while the harder bottom layers will ensure good load bearing capability. From literature review, it is found that carbon-alloyed TMDs with graded structure has not yet been extensively studied. As such, in this thesis, the tribological performance of this graded structure will be specifically analyzed and compared against coatings with a conventional structure.

5. Objective

The objective of this master thesis is to investigate the tribological performance of three types of carbon-alloyed WS_2 coatings. These coatings are W-S-C with 50 at.% C, 35 at.% C and one with a graded structure. The tribological performance will be assessed under room temperature (ambient conditions), dry N_2 environment, and at elevated temperature (ambient air). The steps to be executed to accomplish the objective is as follows:

1. Deposit W – S – C coatings (50 at.%, 35 at.%, and graded composition).
2. Study the properties and performance of the deposited W – S – C coatings.
3. Perform surface characterization on the deposited W – S – C coatings.
4. Perform a series of tribological tests on the W – S – C coatings under different environments.
5. Compare the surface characteristics and tribological performance of the reference W – S – C coating with 50% at. of C, a W-S-C coating with ~35 at.% of C and a coating with a graded composition/structure.

6. Experimental Part

6.1 Coatings Deposition

There are three types of coatings that are examined in this study. The first coating is a W-S-C coating with ~50 at.% carbon content which serves as a reference coating. The second coating is a W-S-C coating with ~ 35 at.% carbon content. The last coating is a W-S-C coating with a graded structure. The graded structure has carbon-rich bottom layers and possesses layers gradually decreasing carbon content that finishes with pure WS_2 on the top layer.

Figure 5. Deposition chamber from Teer Coatings Ltd.

UDP 650/4 Teer Coatings deposition equipment, a DC closed field unbalanced magnetron sputtering system, was utilized to deposit the coatings on top of M2 steel substrates and single crystal silicon wafers. The M2 steel substrates were polished to a 3µm diamond finish (R_a < 20nm), ultrasonically cleaned for 15 minutes each in acetone and ethanol and air-dried before placing them on a rotating fixture in the chamber. The rotating fixture was placed at a target to substrate distance of ~ 25 cm. Two graphite (99.99%), one WS_2 (99.99%), and one Cr targets are mounted on the magnetrons inside the chamber. The chamber is pumped-down to a pressure of < 5 x 10^{-4} Pa. Before the deposition of the coating, the targets and the samples were cleaned

simultaneously. The targets were sputter cleaned in pairs for 20 minutes each pair. For example, first the WS_2 and one of the graphite targets were cleaned for 20 minutes with shutters in front of them to prevent cross-contamination. Then, the shutter is placed in front of the other pair of targets (Cr and graphite) and those targets are cleaned for 20 minutes. The targets are supplied with DC current (Advanced Energy Pinnacle) at a power of 1000 W. During the cleaning of the targets, the substrates are also sputter cleaned using a p-DC voltage (Advanced Energy Pinnacle Plus) of 600 V (resulting in ~1000 W of power). As the substrates are sputter cleaned simultaneously with the targets, the sputter cleaning for them lasts for 40 min.

The deposition of a chromium interlayer was done by bringing the power to Cr target to 2000 W and applying a substrate bias of 110 V. After 10 minutes, a chromium interlayer was formed at 300-400 nm thickness. This interlayer would serve to promote adhesion between the substrate and the W-S-C coating. Once the chromium interlayer was deposited, the deposition of a gradient layer would follow. This was done by reducing the power to the Cr target and increasing the power to WS_2 and graphite targets to 1000 W and 1500 W (on each), respectively. After 10 minutes, the power to the Cr target was stopped and power to the WS_2 and graphite targets were kept at 1000 W and 1500 W, which would result in W-S-C coating with ~50 at.%. A W-S-C coating with ~30 at.% was deposited by following the same procedure but the power to WS_2 and graphite targets was set to be 1000 W and 800 W, respectively. The whole coating deposition process took two hours to complete.

The W-S-C coatings with the graded structure were deposited using a different procedure. After the formation of the Cr layer and the gradient W-S-C layer, W-S-C with ~50 at.% content was deposited by keeping the power to 1500W for the graphite targets and 1000W for the WS_2 target for a total of 20 minutes. Then for 20 minutes each, layers of W-S-C with ~40 at.%, ~30 at.%, and ~20 at.% carbon content were deposited by setting the power to graphite targets to 1000W, 750W, and 500W, respectively. Finally, the power to the graphite targets was reduced to 0W while the power to the WS_2 target was kept at 1000W for 20 minutes. By the last step, pure WS_2 top layers would form on the coating. The sequence is also plotted in the following figure for ease of understanding.

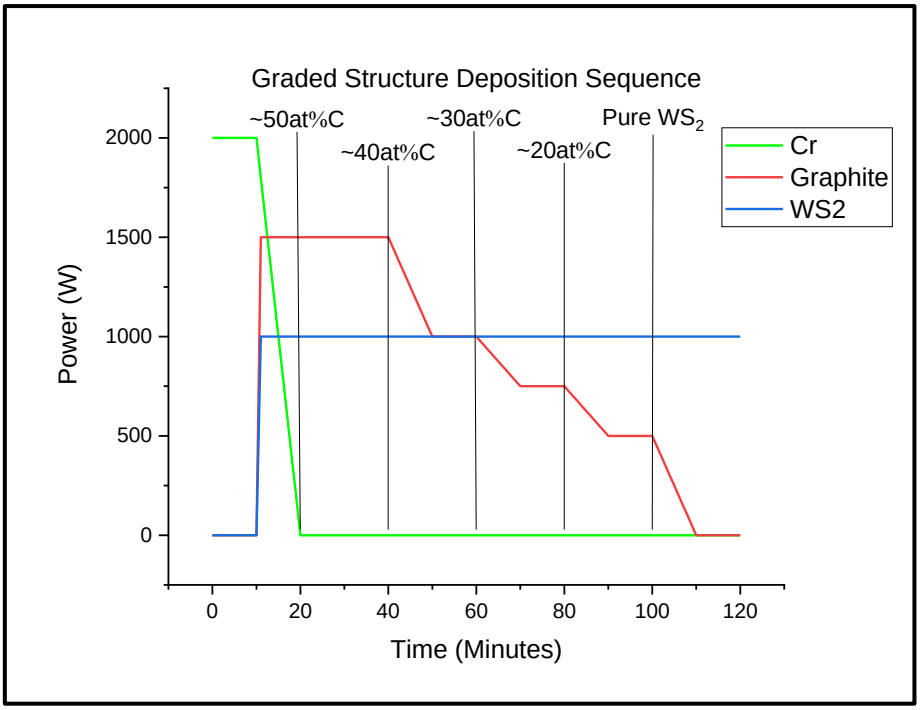

Figure 6. Deposition sequence for coatings with graded structure.

6.2 Characterization Of The Coatings

6.2.1 X-ray Diffraction

X-ray diffraction is a material characterization technique that provides information about the structure of crystalline materials. The technique involves probing a sample material with an X-ray and detecting the resulting diffraction pattern. The diffraction of x-ray occurs because the wavelength of the X-ray source is on the same order of magnitude as the interatomic spacing of crystalline materials. A distinct diffraction pattern is produced when the detector receives a significant constructive diffraction interference signal. This technique would give insight into whether crystalline phases of WS_2 exist on the coatings.

The structural information of the coatings in this study was examined using grazing incidence X-ray diffraction. In grazing incidence X-ray diffraction, the incident X-ray angle is kept small and constant while the detector moves along a measurement circle. This technique is particularly ideal to characterize thin films such as coatings. With this technique, it was expected that the diffraction pattern would contain mostly information on the coating without significant signals from the chromium interlayer. The x-ray diffraction was conducted using Philips X-Pert Pro MPD diffractometer with cobalt as the x-ray source ($\lambda = 1.79$ Å). The angle of detection was set from 5° to 90° while the incident angle was kept at 2°.

6.2.2 Raman Spectroscopy

Raman spectroscopy is a technique that utilizes the interaction of monochromatic light with matter to obtain information of the molecular vibrations which can be exploited for sample identification and quantification. This spectroscopic technique can particularly be used to find out information about the sample materials' chemical structure, phase, and crystallinity. For W-S-C coatings, Raman spectroscopy can even reveal the presence of crystalline WS_2 that is too small for x-ray diffraction analysis to detect [24], [25], [33].

In this study, micro-Raman analysis of the coatings as deposited were performed using Horiba HR800 spectrometer with an acquisition time of one minute. A backscattering configuration with 600 lines mm^{-1} grating and 441.6 nm laser from Kimmon IK Series HeCd laser was employed. An ND1 filter was used in order to reduce the intensity of the beam and thus prevent damage to the coatings. The objective used was a 100x one with a numeric aperture of 0.9, which would result in a laser spot size of ~1 μm. A Peltier cooled CCD sensor would be utilized to collect the backscattered Raman radiation.

6.2.3 Scanning Electron Microscopy and Wavelength-Dispersive Spectroscopy

Scanning electron microscopy (SEM) is a characterization technique employed to examine the morphology of a material. This technique uses electrons as a probe and the resulting secondary electrons and backscattered electrons are captured by a detector. The output of SEM is a micrograph that possesses information regarding a sample material's morphology which contrasts the local topology and atomic weight. For this study, SEM would be used to study the coatings' morphology from the top and the cross-section.

The incident electron beam from SEM also generates characteristic x-rays from the sample which can be captured by a detector for further analysis. Wavelength-dispersive spectroscopy (WDS) examines the wavelength of the generated x-ray to identify the chemical elements present in the sample. In this study, WDS would be used to determine the composition of the coatings by the atomic percentage of the elements. This data would also be utilized to determine the sulfur-tungsten ratio of the coatings.

Field emission SEM (Zeiss Merlon) was employed to obtain the micrographs of the top and the cross-section of the coatings. The chemical composition of the coating was studied by the mounted WDS equipment on the SEM.

6.2.4 Nanoindentation

Nanoindentation is a widespread technique to assess the mechanical properties of a surface. This technique is especially common for the determination of local hardness and elastic modulus of a surface. Typical nanoindenter equipment applies and measures mechanical load and indenter displacement via sensors and actuators. The indenter tip is usually made of diamond. In a nanoindentation experiment, the indenter tip is pressed against the surface at specified loading and unloading profiles [34]. The resulting load-displacement curve is recorded and studied. The hardness value is determined by dividing the maximum applied load by the indentation area before unloading.

In this study, nanoindentation experiments was done using NanoTest platform from MicroMaterials Ltd. This equipment possesses a diamond tip with a Berkovich pyramid shape. The load was set to 3 mN, which resulted in indentations within 10% of the coatings' thickness.

6.2.5 Scratch Test

Sufficient adhesion to its substrate is imperative for the practicality of the coating. However, there is no one test to assess the adhesion that is applicable for all coating-substrate systems. This is because all known adhesion testing methods are affected not only by the coating adhesion but also by other properties of both the coating and the substrate [35]. The adhesion of the coatings in this study was assessed by a scratch test as depicted in figure 7, where a hard indenter would be pressed and slid against the coatings with a specified loading rate. The resulting scratch on the surface is then analyzed by an optical microscope to identify the failure events. The failure events would be related to the critical loads at which the failure events started to occur. The critical loads Lc_1, Lc_2, and Lc_3 represent the loads at which cracks start to form, chipping on the border of the scar and/or interfacial spallation, and gross delamination of the coating, respectively [36].

The scratch test was performed by the Revetest tool from CSEM instruments. The indenter used was a Rockwell C diamond indenter with a 0.2 mm tip radius. The loading rate used was 10 N/mm that started at 2N and ended at 70N.

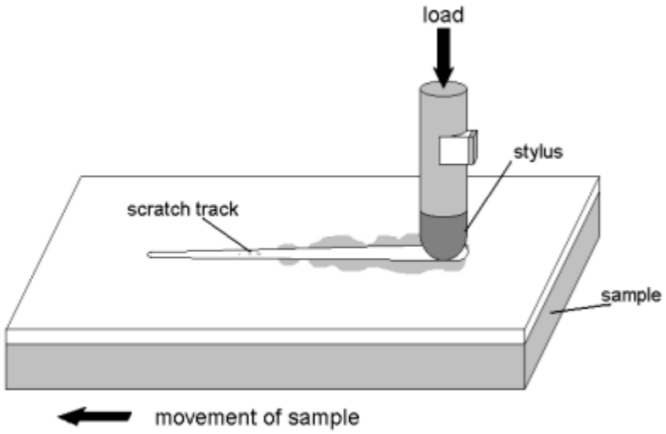

Figure 7. A diagram of a typical scratch testing [37].

6.3 Tribology Experiments

The coatings' tribological performance was assessed by a reciprocating ball-on-disk tribometer (Optimol SRV) using a DIN 100Cr6 steel ball with a10mm diameter as the counterbody. The counterbody was pressed against the coating with a 10 N force. The stroke and the oscillation of the counterbody were set to be 2 mm and 10 Hz, respectively. The test duration was set to 20 minutes or until a catastrophic failure of the coatings occurred. The tribometer set up is depicted in figure 8.

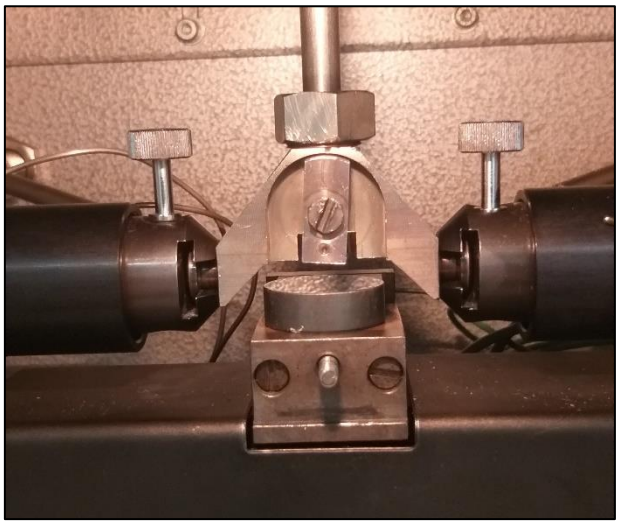

Figure 8. Tribotester set-up that is employed for the experiments.

The tribological performance was examined under three environments, namely, under ambient environment, under dry nitrogen gas environment, and at elevated temperature. Under a dry N_2 environment, the chamber was subjected to a constant flow of N_2 gas, and the relative humidity inside the tribometer chamber was measured by a hygrometer. For every dry N_2 experiment,

the relative humidity inside the chamber was always lower than 7 %. For elevated temperature experiments, the stage on which the coated samples were placed was heated to 200 °C.

Table 1. Parameters of reciprocating tribometer experiments.

Applied Load (N)	10
Stroke (mm)	2
Frequency (Hz)	10
Speed (m/s)	0.04
Duration (s)	1200
Total sliding distance (m)	48

The tribological performance of the coatings was assessed in terms of coefficient of friction evolution of the system and wear assessment. After each experiment, the wear scars of the coating and the ball counterbody was taken under Alicona InfiniteFocus™ 3D profilometer with 100X objective (which results in a vertical resolution of 20nm) to analyze their dimensions. The wear volume was calculated using the equation as suggested by ASTM G133 – 05 standard [38]:

$$W_v = W_q * s$$

Where W_v, W_q, and s are the wear volume, cross-sectional profile of the wear area, and the stroke, respectively. Then, the specific wear rate can be calculated using the equation below:

$$W_r = \frac{W_v}{F * d}$$

Where W_r, F, and d are the specific wear rate, the applied normal load, and the total distance traveled, respectively. The wear volume of the ball counterbody was taken as a spherical cap and calculated using the following formulas:

$$V_{ball} = (\frac{\pi * h}{6})(\frac{3d^2}{4} + h^2)$$

$$h = r - \sqrt{r^2 - \frac{d^2}{4}}$$

Where h, r, and d represent the height of the spherical cap, the radius of the ball, and the scar diameter, respectively. Once the wear volume of the ball was obtained, it was also normalized by the applied force and total distance traveled to obtain the specific wear rate of the ball.

7. Results and Discussion

There are three types of coating that are examined in this study. In this section, WSC35 refers to W-S-C coating with ~35 at.% carbon content, WSC50 refers to W-S-C coating with ~50 at.% carbon content, and WSCG1 refers to W-S-C coating with the graded structure. The results from the experimental parts will be presented using the label for consistency.

7.1 Chemical composition, microstructure, and crystallinity

The table below shows the actual chemical composition of the coatings as deposited obtained via WDS.

Table 2. Chemical composition of the deposited coatings.

Coating	Chemical composition (atomic percentage)				S/W Ratio
	S	W	O	C	
WSC50	28.93 ± 0.22	20.29 ± 0.04	2.70 ± 0.03	47.84 ± 0.22	1.43
WSC35	35.37 ± 0.19	24.90 ± 0.18	3.46 ± 0.08	36.14 ± 0.29	1.42
WSCG1	52.48 ± 0.04	36.07 ± 0.08	4.43 ± 0.17	6.82 ± 0.03	1.45

Much like the microstructure and mechanical properties of TMD coatings deposited by sputtering techniques, the chemical composition of the coatings is also largely affected by the deposition parameters [24], [25], [39]–[41]. As shown in the table, all coatings had a similar S/W ratio of about 1.4. This is because the parameters of importance that directly alter sulfur content are the target-substrate distance and the argon pressure inside the deposition chamber [25], [40], [41]. These parameters were not varied during the deposition process of the coatings. However, coatings with low S/W may still serve as a good low-friction coating as long as the tribofilm that is formed on contact is not severely worn away [42].

WSC50 and WSC35 had carbon content of ~48 at.% and ~36 at.%, respectively. The reduction of carbon content from WSC50 to WSC35 served its intended purpose, as the S and W contents of the coatings increased from 28 at.% and 20 at.% to 35 at.% and 25 at.%, respectively. All coatings also showed a trace amount of contaminant oxygen, though it was not expected to affect the tribological performance of the coatings. The WDS analysis was performed on the

top surface of the coatings. Therefore, it only detected around 6.8 at.% of carbon in the WSCG1 sample.

Micrographs of the samples obtained from SEM analysis confirmed that the coatings were about 1.5 μm thick. The chromium interlayer in the samples was approximately 300 nanometers. Micrographs of WSC50, WSC35, and WSCG1 can be observed in figures 9,10, and 11, respectively. The chromium interlayer is observed to be notably columnar. On the other hand, the cross-section of the W-S-C layers in each coating displays compact structures without significant porosity. This implies better mechanical properties when compared to a coating with pores and columnar features. The top view of WSC50 and WSC35 coatings showed a cauliflower-like structure that is typical of W-S-C coatings deposited by magnetron sputtering. The same pattern could be recognized on WSCG1 coating, though much less pronounced since the top layer of WSCG1 is virtually a pure WS_2. The cross-section micrograph of WSCG1 also exposed the distinct top layer of WS_2, which was measured to be around 150 nanometers thick. Much like the chromium interlayer, the top layer of WSCG1 manifested a columnar structure.

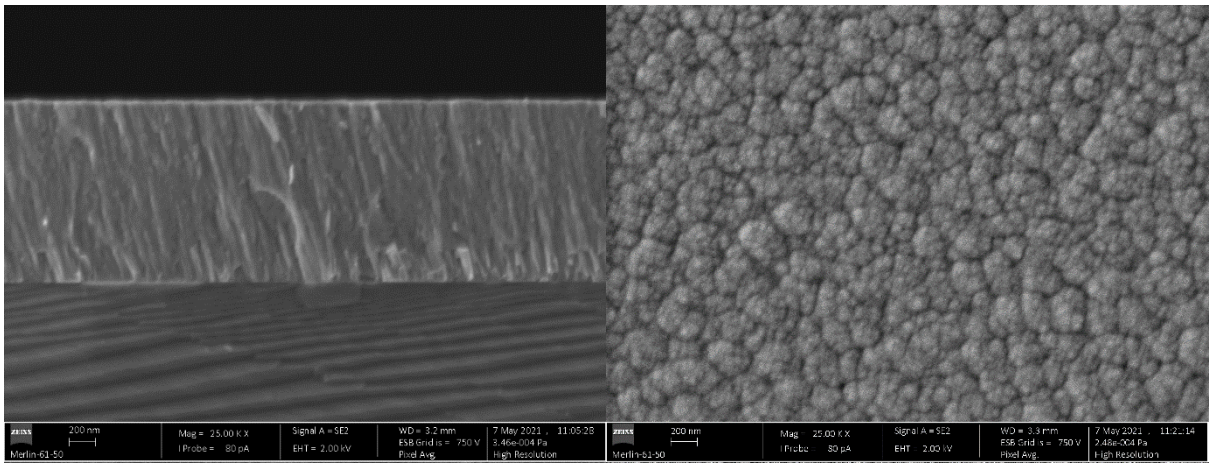

Figure 9. SEM micrographs of WSC50, cross-section view (left) and top view (right).

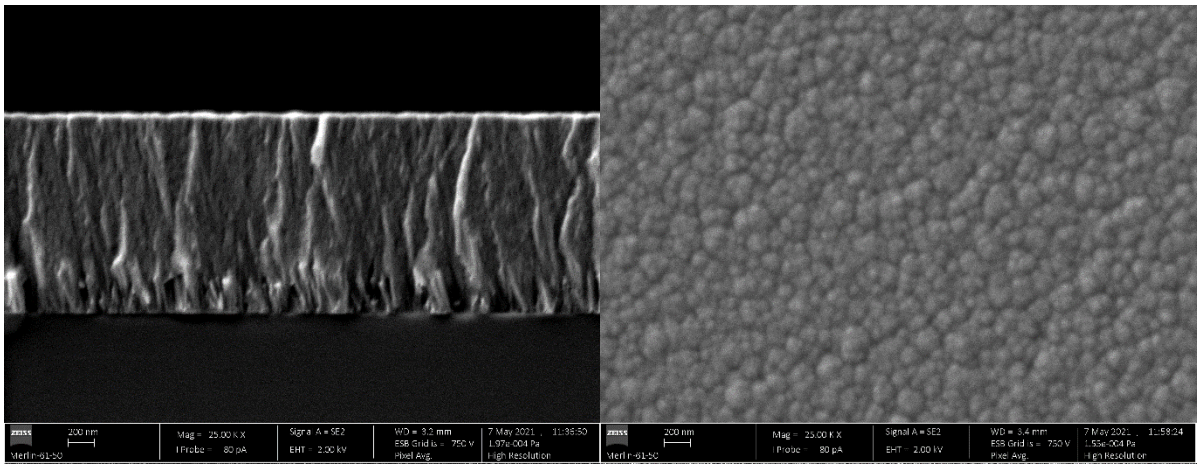

Figure 10. SEM micrographs of WSC35, cross-section view (left) and top view (right).

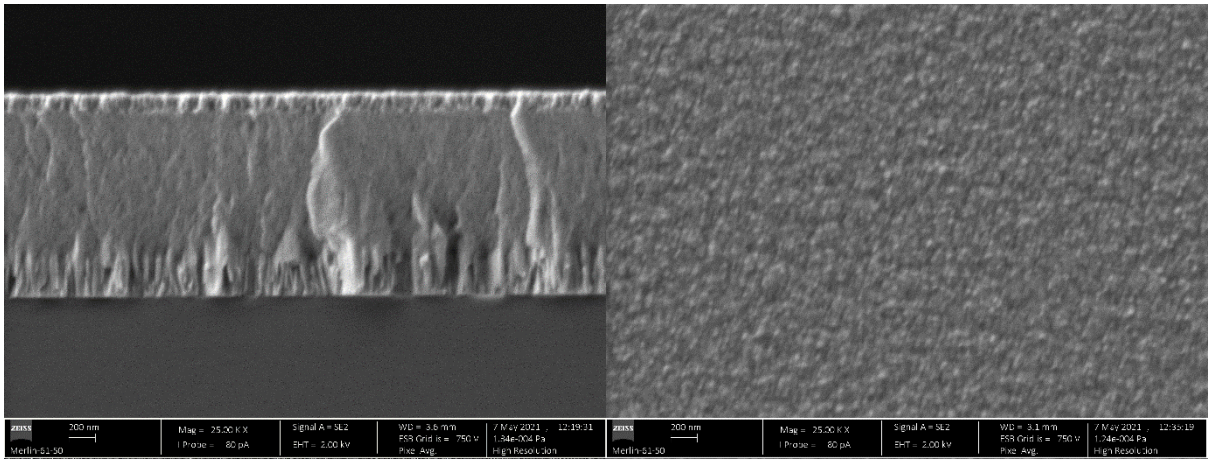

Figure 11. SEM micrographs of WSCG1, cross-section view (left) and top view (right).

The diffractograms of the coatings obtained from the grazing incident x-ray diffraction analysis are observed in figure 12. As expected, only WSCG1 shows sharp peaks belonging to WS_2 crystalline phase since it was the only coating that possesses pure WS_2 crystals on the top layer. There were three observable peaks that correspond to (002), (100), and (110) WS_2 phases in WSCG1 (ICDD Ref No: 01-084-1398). The observed peaks were not exactly on the same positions stated by the ICDD card, which indicated a different interplanar distance of WS_2 crystals. This can be attributed to the fact that the S/W ratio in the coatings are not exactly 2. The presence of (002) peak indicate that the basal plane of some of the WS_2 crystals were oriented parallel to the substrate and thus to the sliding direction [43]. This orientation was most preferred for superior tribological performance as it would lead to the lowest COF and wear, compared to other orientation. However, it must be noted that with the presence of (100) peak, the basal planes of some WS_2 crystals in WSCG1 were oriented perpendicular to the substrate [43].

With increasing carbon content, W-S-C system is expected to retain amorphous structures [44]. Broad peaks observed in WSC50 and WSC35 diffractograms between 2θ of 30° to 55° indicate significant amorphous phases. Several peaks within this amorphous area have been attributed to WS_2 and WC planes [24]. Peaks belonging to chromium are not detected in the diffractogram indicating that the GIXRD experiments did not penetrate deep into the coating.

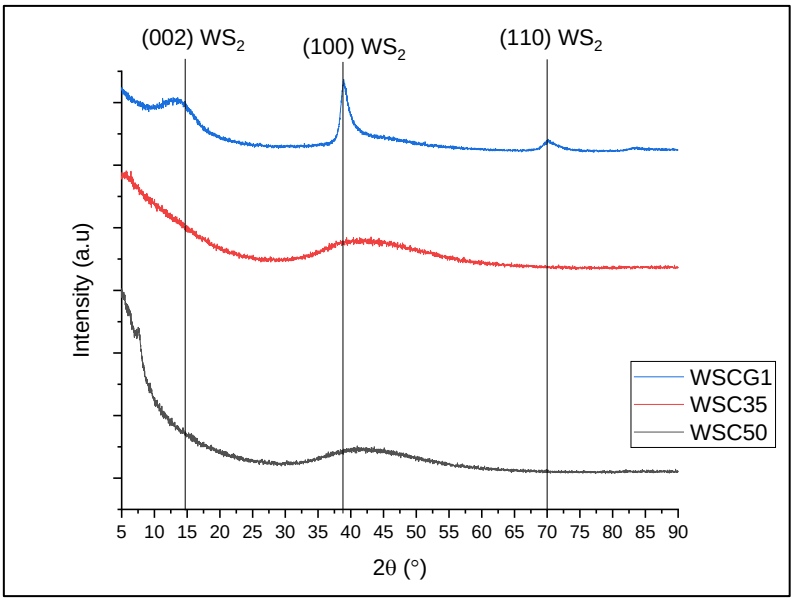

Figure 12. X-ray diffractogram of the deposited coatings.

The results of Raman spectroscopy analysis for all coatings as deposited can be studied in figure 13. The vibration modes of WS_2 are identified from peaks at ~180 cm^{-1}, ~360 cm^{-1}, and ~418 cm^{-1} [45]. The Raman spectra of the coatings show intense peaks at ~360 cm^{-1} and ~418 cm^{-1}, further confirming the presence of rich crystalline WS_2 top layers. No peaks related to WS_2 were observed in both WSC50 and WSC35 Raman spectra, indicating reduced crystallinity and the amount of the WS_2 phase.

Another element of interest in W-S-C coating system is graphitic carbon. The presence of graphitic carbon can be observed by its D and G modes of vibration which are located at around 1350 cm^{-1} and 1580 – 1600 cm^{-1}, respectively [46]. Though the peaks for both graphitic carbon's modes of vibration could be observed in all coatings' Raman spectra, their positions were shifted and dispersed, especially in WSC35 and WSC50 Raman spectra. This observation indicated that the carbon phase in the coatings manifested an amorphous structure [46].

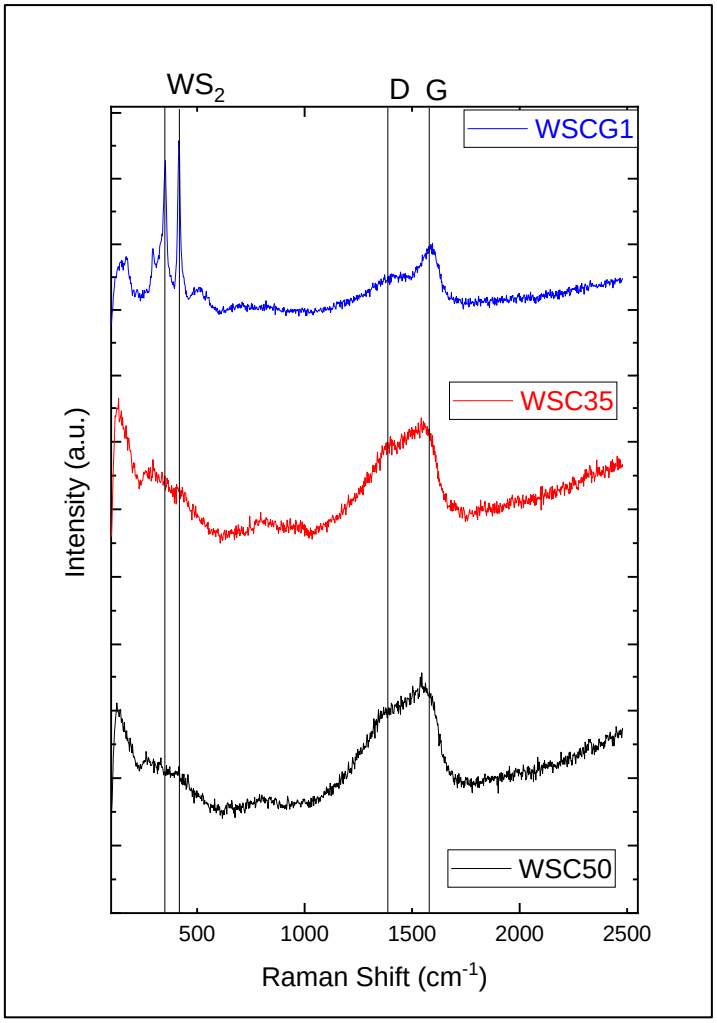

Figure 13. Raman spectra of the coatings.

7.2 Mechanical Properties

Figure 14 shows the hardness values and the reduced Young's moduli of the deposited coatings from nanoindentation with 3 mN load. Nanoindentation tests with 1 mN load was also performed, but the results were similar to the 3 mN tests. The mechanical properties of W-S-C coatings are affected by two factors, namely, the carbon content and the S/W ratio [24]. A WS_2 film by itself is soft. When alloyed with carbon, the film underwent changes to its morphology to form a compact film, as opposed to a columnar morphology with pores [47]. This morphological change contributed to the improvement of mechanical properties from pure WS_2 to W-S-C. Furthermore, with the addition of carbon, there is the possibility of formation of tungsten carbide phases, which are inherently harder than tungsten disulfide [47]. A low S/W ratio generally implies a greater amount of tungsten to form the hard WC phases in the coating.

Having the greatest amount of carbon content, WSC50 possessed the highest hardness and reduced modulus values among the coatings at roughly 6.42 ± 0.23 GPa and 93.42 ± 2.00 GPa,

respectively. At reduced carbon content of ~35 at.%, WSC35 had a hardness of 5.62 ± 0.31 GPa and reduced modulus of 89.20 ± 3.13. Though WSCG1 had decreasing carbon content on its upper layers, the coating's mechanical properties were still competitive. This is because the indentation depth measured was ~150 nm. As such, the hardness response of WSCG1 coating came from the bulk of the coating which had significant carbon content. The hardness and reduced modulus of WSCG1 were 5.58 ± 0.26 GPa and 91.5 ± 3.24 GPa, respectively.

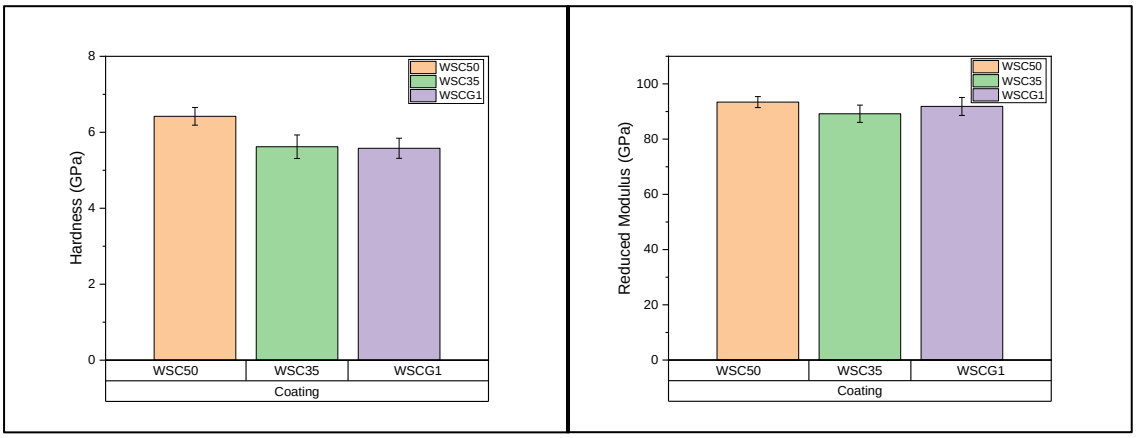

Figure 14. Hardness (left) and reduced modulus (right) data of the deposited coatings.

7.3 Scratch Test

The result of scratch tests is summarized in table 3. The scratch tracks themselves can be investigated from figures 15, 16, and 17 for WSC50, WSC35, and WSCG1, respectively. The first critical load, Lc_1, shows that the harder coating (WSC50) resisted cracking better than the softer ones (WSC35 and WSCG1). WSC50 experienced the second failure event, chipping and spalling on the border of the scratch scar, fairly quickly at ~17 N. Finally, gross delamination could be observed on WSC50 after the application of ~36 N load.

WSC35 resisted spallation and chipping better than WSC50. The second critical load for WSC35 was ~22 N. During the second failure event, chipping within the scratch scar was also observed on the WSC35 coating. Gross delamination of WSC35 coating could be observed at a lower applied force than WSC50 at 26 N. The result of scratch tests cannot be conclusive to determine if lower carbon content produces a coating with better adhesion. However, the results show that the coating with lower carbon content has a different failure mechanism, i.e. it is more susceptible to delamination than chipping or spallation.

Though the initial cracking load was the lowest for WSCG1, the coating actually performed the best for the subsequent failure events. Its second critical load was highest at ~28N. Gross delamination was not observed on the scratch scar of the coating, which indicated superior adhesion to the substrate. The scratch scar of WSCG1 also appeared considerably smoother compared to the scratch scars belonging to WSC50 and WSCG1. This observation was not unexpected since the top layer of WSCG1 was rich in pure, crystalline WS_2 which was easily sheared.

Table 3. Critical loads of the coatings obtained from scratch tests.

Coating	Lc_1 (N)	Lc_2 (N)	Lc_3 (N)
WSC50	8 ± 1	17 ± 1	36 ± 1
WSC35	6 ± 1	22 ± 1	26 ± 1
WSCG1	4 ± 1	28 ± 1	-

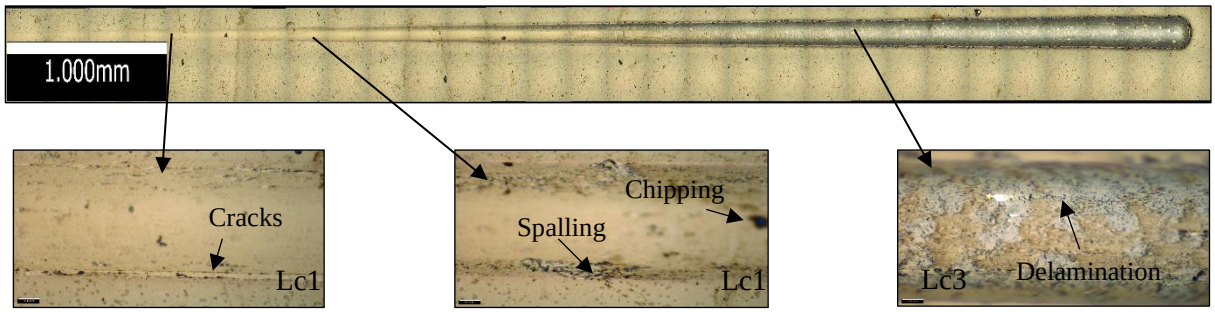

Figure 15. Scratch test result for WSC50.

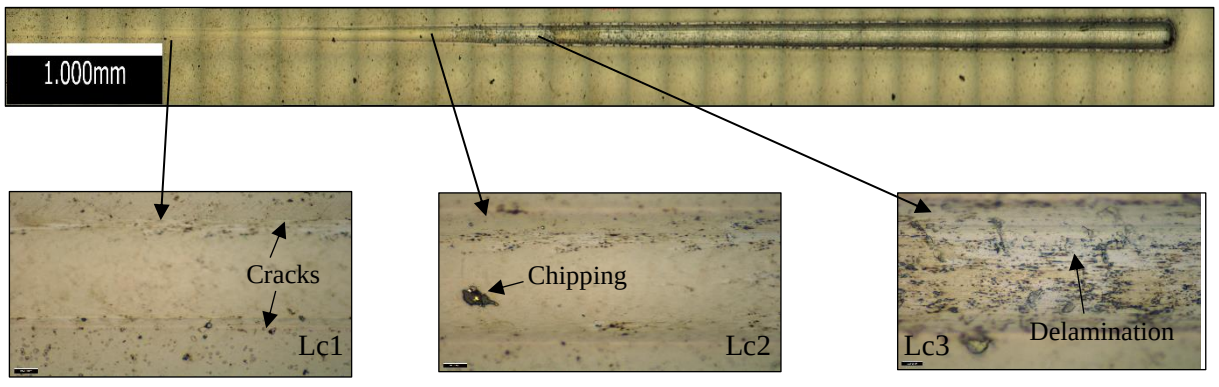

Figure 16. Scratch test result for WSC35.

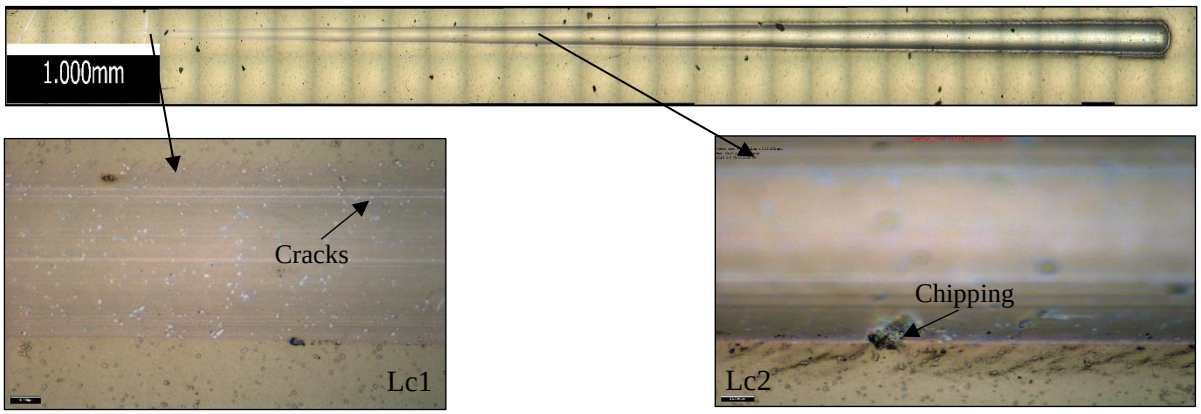

Figure 17. Scratch test result for WSCG1.

7.4 Tribological Performance

As mentioned previously, the tribological performance of the coatings was assessed under three conditions, namely, under ambient air at room temperature, under dry N_2 environment (room temperature), and under elevated temperature at 200°C. The purpose of varying test conditions is to deduce the most flexible self-adaptive low-friction coating. The results of the experiments will be discussed in the following sections.

7.4.1 Room temperature experiments

As observed in figure 18, in the room temperature experiments, both WSC50 and WSC35 reached steady-state coefficients of frictions of around 0.10 and 0.13, respectively. It is established that at room temperature, the carbon phases of the coating regulates the lubrication via graphitization [19], and the role of the WS_2 phases is considered minor. As such, having a significant amount of carbon phases, WSC50 and WSC35 managed to produce low and stable coefficients of friction. Additionally, the WSC50 coating had a superior hardness and modulus which affected its wear resistance. In this context, it is expected for the friction pair with superior wear resistance to have a lower COF as wear as a process is dissipating energy. Additionally, based on the Bowden and Tabor theory for metallic friction, the best sliding scenario would be to have a low shear strength interface supported by an underlying phase with higher hardness [16]. If the shear strength of the interface is similar in both WSC50 and WSC35 coatings, it is expected that WSC50 to show a lower COF due to the higher hardness of the load supporting phase. WSC50's superior performance over both WSC35 and WSCG1 was

also reflected in its low coating and ball specific wear rates at ~2.36 × 10^{-7} mm^3/Nm and ~2.13 × 10^{-8} mm^3/Nm, respectively. The coating specific wear rates for WSC35 and WSCG1 were greater than double than that of WSC50 at ~5.45 × 10^{-7} mm^3/Nm and ~4.96 × 10^{-7} mm^3/Nm, respectively. The ball specific wear rates for WSC35 and WSCG1 were ~6.39 × 10^{-8} mm^3/Nm and ~7.26 × 10^{-7} mm^3/Nm, respectively.

WSCG1 yielded a fluctuating coefficient of friction throughout the full 20 minutes of the test. The initial steep drop of coefficient of friction of WSCG1 from ~0.14 to ~0.08 was likely the result of the reorientation of the basal planes of pure WS_2 crystals in the top layers of the coating. It must be noted, however, that WS_2 has reduced lubrication capability in humid environments because it is susceptible to oxidation and has a higher shear-strength in the presence of humidity [48], [49]. Due to the reduced content of carbon phases on the top layers, the coating could not reach a steady-state coefficient of friction. Even so, WSCG1 did not show signs of catastrophic failure in the experiments since the coefficient of friction would always drop after a spike, and it never exceeded the initial running-in coefficient of friction. Nevertheless, even though WSCG1 did not settle to a stable coefficient of friction, its wear rates for the coating and the ball counterbody were very comparable to WSC35 coating.

Measurements from 3D optical microscopy showed that the wear depth of WSCG coatings reached ~600 nm, which was far greater than the thickness of the pure WS_2 top layer. This supported the idea that even though the top layer could provide low friction, it was easily worn away, and thus the coefficient of friction would increase. Once the counterbody wore enough of the top layer and reached layers with a greater amount of carbon phase, the wear would slow down and a friction-induced crystallization of WS_2 phases would be formed on the contact once more. This repeated wear and formation of the lubricous tribolayer was responsible for the fluctuating coefficient of friction in the WSCG1 system.

The wear scars of the coatings and their accompanying wear height profile can be observed in figures 19, 20, and 21. The wear scar of WSCG1 was noticeably different compared to the wear scars of WSC50 and WSC35 as it possessed a distinctly blue outline surrounding the scar. Knowing the composition of WSCG1, it is deduced that the blue outline was the pure WS_2 materials that had been smeared away from the contact. On the other hand, the wear scars of WSC50 and WSC35 appeared alike, with smooth scars and little amounts of debris on contact. The measurements from 3D optical microscopy show that while the wear depth of WSC35 reached similar values as WSCG1, the scar was considerably narrower, resulting in a much

lower wear volume. As for the WSC50 wear scar, its depth was observed to only about ~200 nm deep.

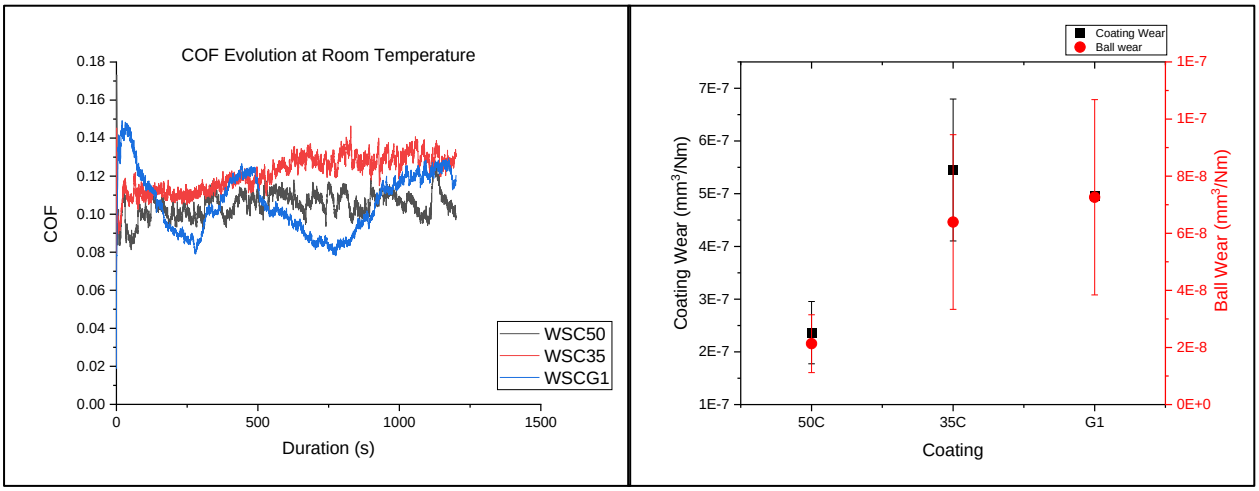

Figure 18. Friction evolution and specific wear rate of the coatings from room temperature experiments.

Table 4. Specific wear results from room temperature experiments.

Coating	**Coating Wear (mm^3/Nm)**	**Ball Wear (mm^3/Nm)**
WSC50	$2.36 \times 10^{-7} \pm 5.90 \times 10^{-8}$	$2.13 \times 10^{-8} \pm 1.01 \times 10^{-8}$
WSC35	$5.45 \times 10^{-7} \pm 1.35 \times 10^{-7}$	$6.39 \times 10^{-8} \pm 3.06 \times 10^{-8}$
WSCG1	$4.96 \times 10^{-7} \pm 2.36 \times 10^{-9}$	$7.26 \times 10^{-8} \pm 3.24 \times 10^{-8}$

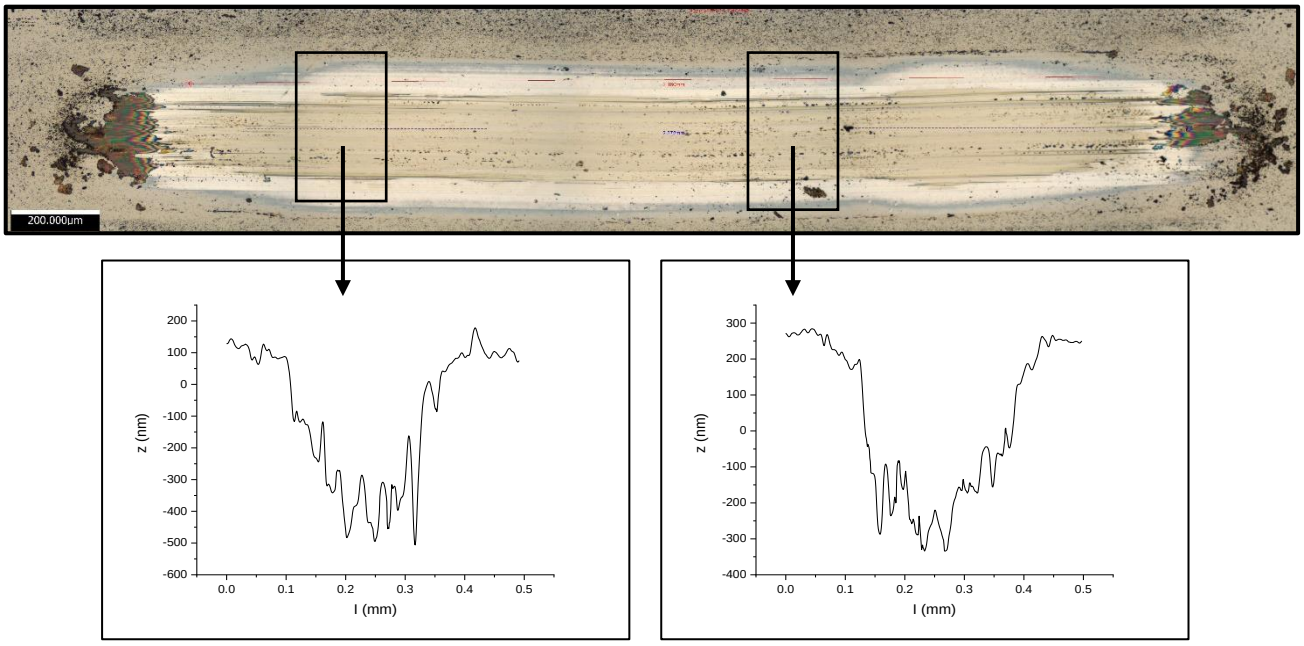

Figure 19. Wear track image of WSCG1 with sample depth measurements from 3D optical microscopy from room temperature experiments.

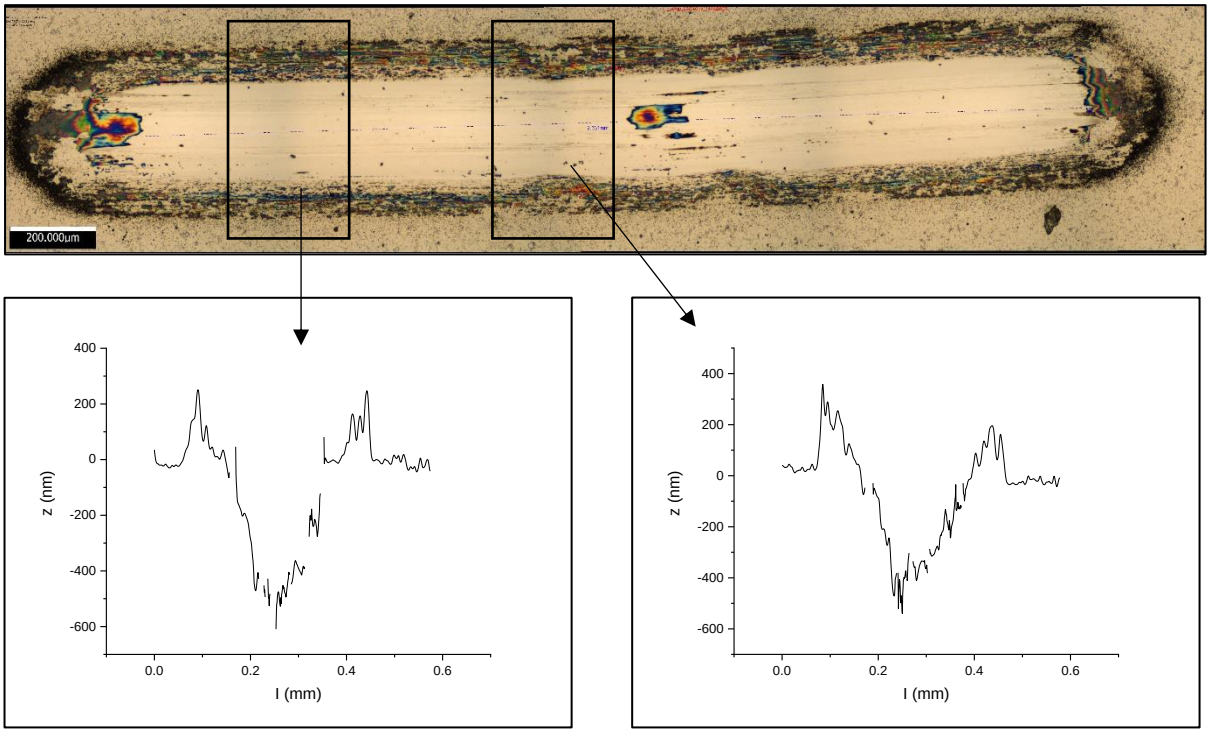

Figure 20. Wear track image of WSC50 with sample depth measurements from 3D optical microscopy from room temperature experiments.

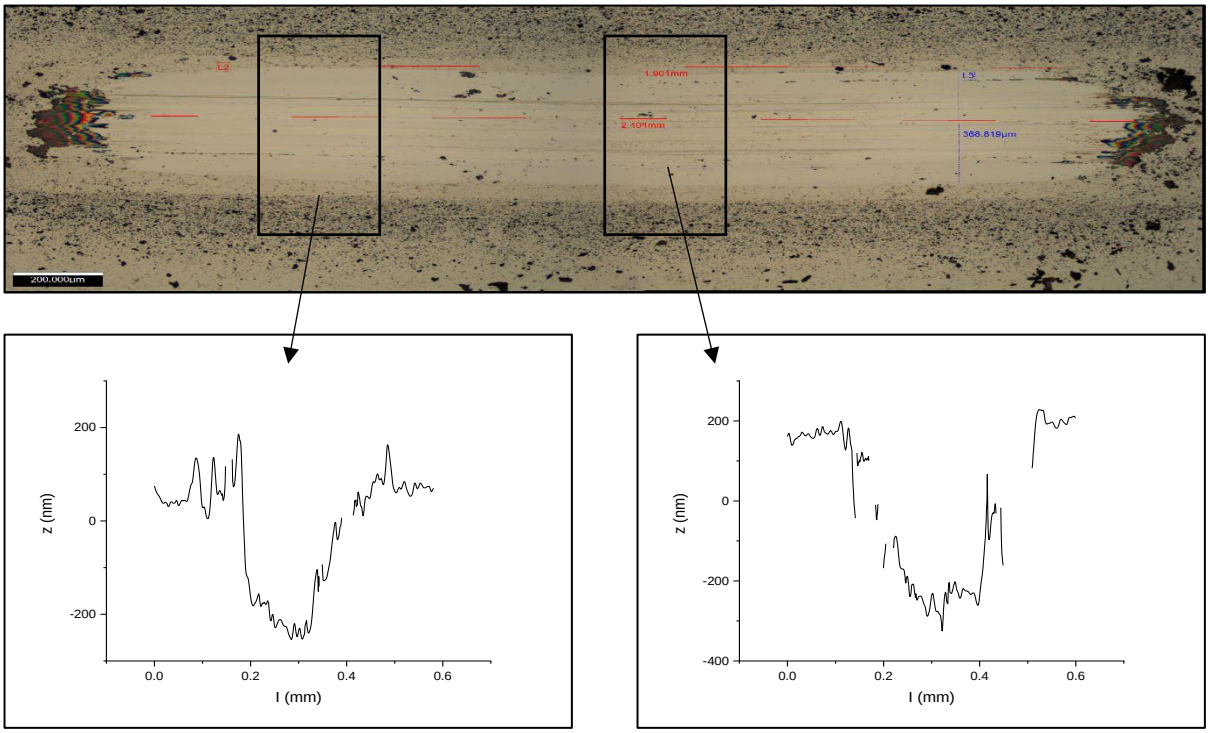

Figure 21. Wear track image of WSC35 with sample depth measurements from 3D optical microscopy from room temperature experiments.

7.4.2 Dry N_2 experiments

The COF evolution in dry in dry N_2 experiments is shown in figure 22. WSC35 and WSCG1 came to steady-state coefficients of friction in the first minutes of the tests. WSC50 took a slightly longer time, which was about 7 minutes, to arrive at steady coefficient friction. WSC50, WSC35, and WSCG1 reached ~0.04, ~0.03, and 0.02 coefficient of friction, respectively. In a dry N_2 environment, the WS_2 phases of the coatings dominate the lubrication mechanism [19]. Therefore, having the highest amount of readily available WS_2 crystals, WSCG1 reached the lowest steady-state coefficient of friction. In contrast, with the highest amount of carbon content, WSC50 expectedly produced the highest coefficient of friction. Even so, all coatings did not experience a spike in the coefficient of friction. The constant coefficients of friction of the systems indicate that once the tribofilm was formed, it remained in contact without being worn away for the full duration of the experiments.

In terms of specific wear rates of both the coating and the ball counterbody, WSC35 and WSCG1 coatings show great improvement from the room temperature experiments. WSC35 produced the lowest specific wear rate for the coating at ~6.67×10^{-8} mm^3/Nm followed closely by WSCG1 at ~1.18×10^{-7} mm^3/Nm. On the contrary, the low coefficient of friction of WSC50 was not accompanied by low specific wear rates of the coating and the ball. Instead, the specific wear rates of both bodies increased considerably from room temperature tests even though the coating resulted in a decidedly lower coefficient of friction.

Figure 23 showed the measurements of the wear scar of WSC50 from 3D optical microscopy. The depth of the wear scar of WSC50 reached deeper than 500 nm. Its width was above 0.3 mm, which was more than double compared to the wear scar of the coating from room temperature experiments. The same measurements for WSC35 and WSCG1 can be obtained from figures 24 and 25, respectively. There was very low amount of wear for both coating as the depth only reached slightly lower than 200 nm for WSC35 and around 200 nm for WSCG1. Though the wear depth was shallow for WSCG1, the top layer rich in WS_2 was still penetrated, albeit just barely.

The wear scars of all the coatings appear smooth as shown in figures 23, 24, and 25. Striations along the direction of the sliding can be observed in all wear scars, though they are particularly well defined on WSCG1 and WSC35. The wear scar of WSCG1 also shows big material smears on both ends of the scar. It must also be noted that the blue material that is present on the wear

scar of WSCG1 from room temperature experiments can be observed in all wear scars from the dry N_2 tests. This fact further supports that the blue-like material is indeed crystalline WS_2.

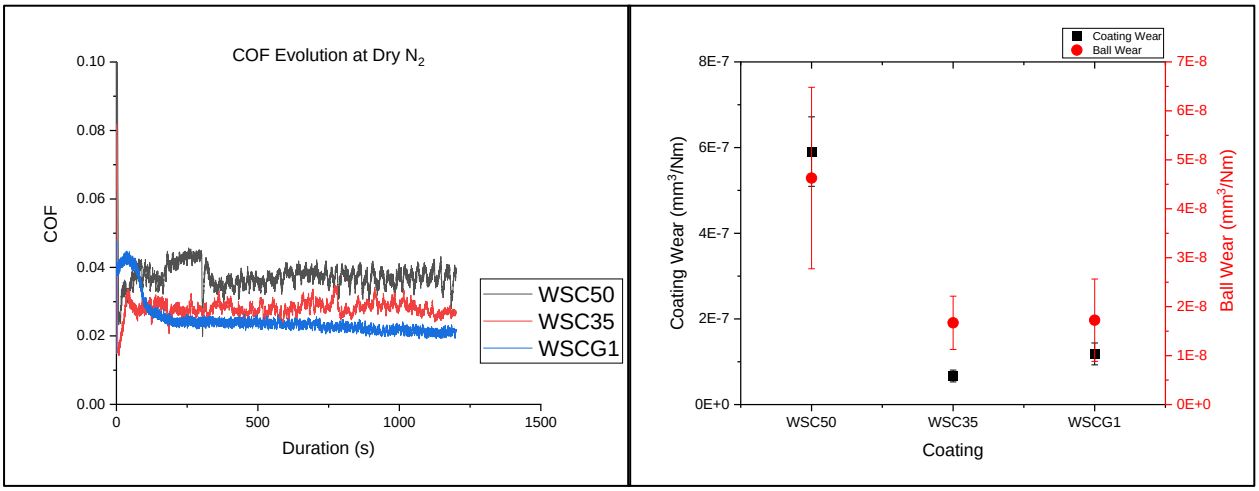

Figure 22. Friction evolution and specific wear rate of the coatings from dry N_2 experiments.

Table 5. Specific wear results from dry N_2 experiments.

Coating	**Coating Wear (mm^3/Nm)**	**Ball Wear (mm^3/Nm)**
WSC50	$5.91 \times 10^{-7} \pm 8.11 \times 10^{-8}$	$4.63 \times 10^{-8} \pm 1.85 \times 10^{-8}$
WSC35	$6.67 \times 10^{-8} \pm 1.37 \times 10^{-8}$	$1.67 \times 10^{-8} \pm 5.44 \times 10^{-9}$
WSCG1	$1.18 \times 10^{-7} \pm 2.56 \times 10^{-8}$	$1.72 \times 10^{-8} \pm 8.41 \times 10^{-9}$

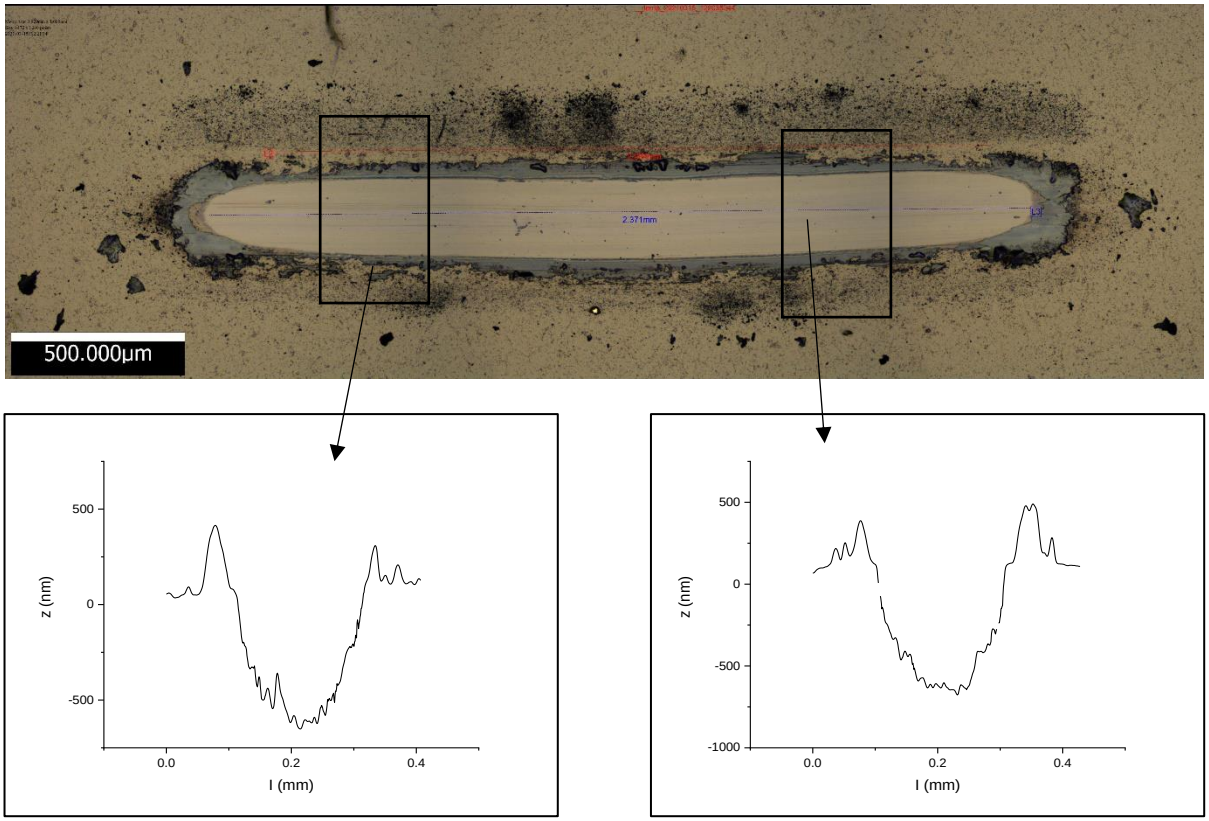

Figure 23. Wear track image of WSC50 with sample depth measurements from 3D optical microscopy from dry N_2 experiments.

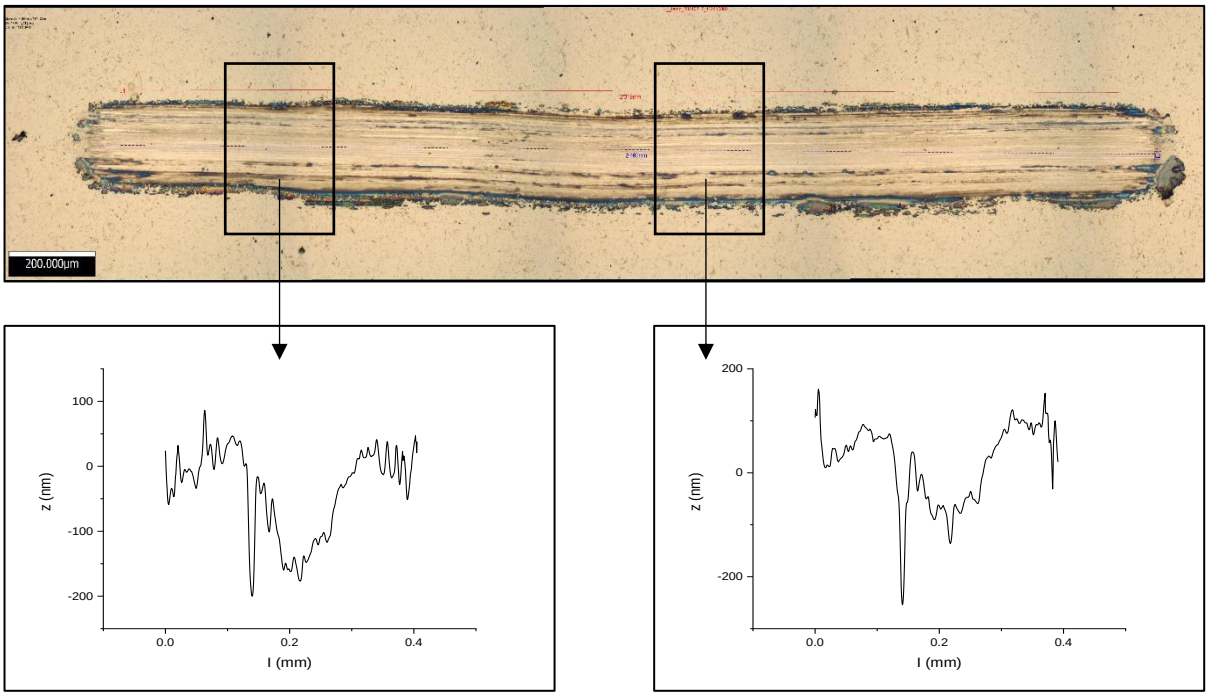

Figure 24. Wear track image of WSC35 with sample depth measurements from 3D optical microscopy from dry N_2 experiments.

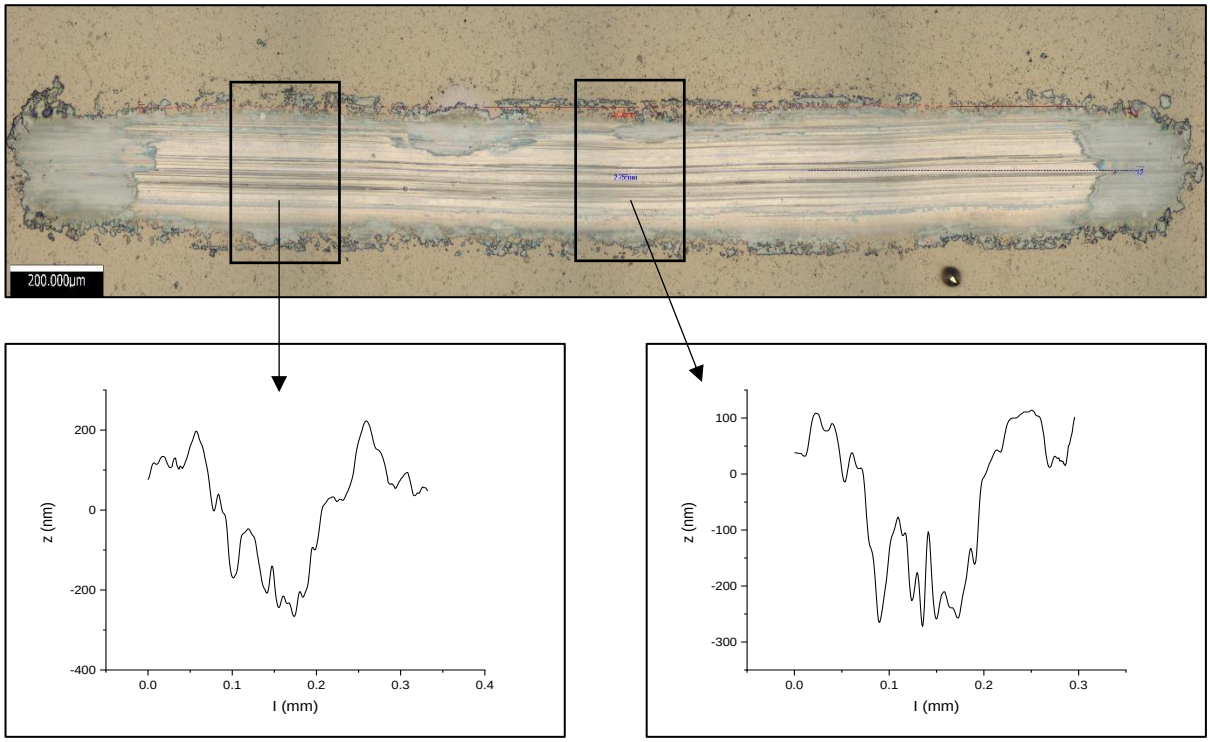

Figure 25. Wear track image of WSCG1 with sample depth measurements from 3D optical microscopy from dry N_2 experiments.

7.4.3 Elevated temperature experiments

As observed in figure 26, all deposited coatings produced their lowest coefficients of friction under an elevated temperature (200°C) condition. Within the first minute of the experiments, the coefficients of friction of all coatings fluctuate between 0.02 to 0.04. As opposed to the other test conditions, there are very minute differences between the steady-state coefficients of friction of the coatings in elevated temperature experiments. For the last minute of the experiment, the coefficients of friction for WSC50, WSC35, and WSCG1 averaged ~0.022, ~0.017, and ~0.024, respectively.

WSC50 and WSC35 yielded the best tribological performance in terms of wear under an elevated temperature condition. The coating and ball specific wear rates for WSC50 are 1.16×10^{-7} mm^3/Nm and 1.25×10^{-8} mm^3/Nm, respectively. For WSC35, the coating and ball specific wear rates are 1.42×10^{-8} mm^3/Nm and ~9.70×10^{-9} mm^3/Nm, respectively. As observed in figures 27 and 28, the measurements of 3D microscopy showed that there was very low wear for WSC50 and WSC35 because the wear depths only reached < 200 nm.

The performance improvement experienced by WSC50 and WSC35 can be attributed to the additional energy provided by the heat that assisted the formation of lubricous crystalline WS_2 [24]. Furthermore, the heat of the system also severely reduced the humidity of the system, thus eliminating a factor that could limit the tribological performance of WS_2 tribolayer [5], [50]. Since the coefficient of friction and the specific wear rates of WSC35 were superior to WSC50, it was gathered that reducing carbon content and subsequently increasing tungsten and sulfur contents of the coating was indeed advantageous.

For WSCG1, the specific wear rates for both the coating and the ball under elevated temperature were higher than those under dry N_2 experiments, even though the coefficient of friction was comparable. The numbers for WSCG1 were 1.84×10^{-7} mm^3/Nm for the coating and ~2.80×10^{-8} mm^3/Nm for the ball counterbody. The measurements of the wear scar obtained by 3D optical microscopy displayed in fig X showed that while the wear depth was still shallow at ~200 nm, it was considerably wider. The width of the wear scar from elevated temperature experiments reached > 0.2 mm whereas the wear scar from dry N_2 experiments was only about ~0.15 mm wide.

As observed in figures 27, 28, and 29, the wear tracks of all coatings showed pronounced striations along the axis of sliding. The black debris on the sliding interface and around the wear scar was highly likely composed of graphitic carbon and tungsten oxide since the added heat input should increase the probability of graphitization and oxidation [24].

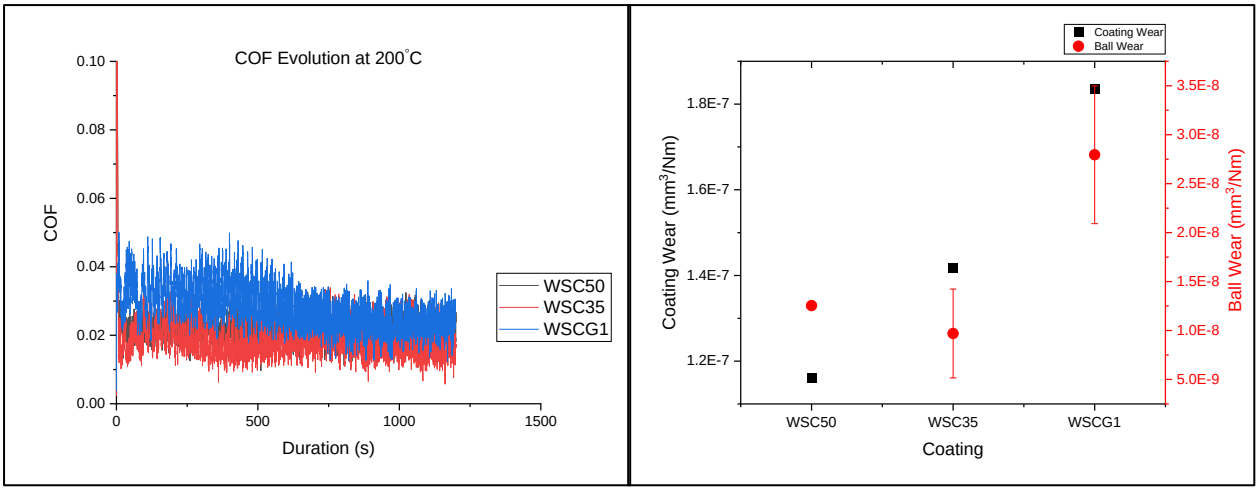

Figure 26. Friction evolution and specific wear rate of the coatings from experiments at 200°C.

Table 6. Specific wear results from elevated temperature experiments.

Coating	Coating Wear (mm^3/Nm)	Ball Wear (mm^3/Nm)
WSC50	1.16×10^{-7}	1.25×10^{-8}
WSC35	1.42×10^{-8}	$9.70 \times 10^{-9} \pm 4.54 \times 10^{-9}$
WSCG1	1.84×10^{-7}	$2.80 \times 10^{-8} \pm 7.03 \times 10^{-9}$

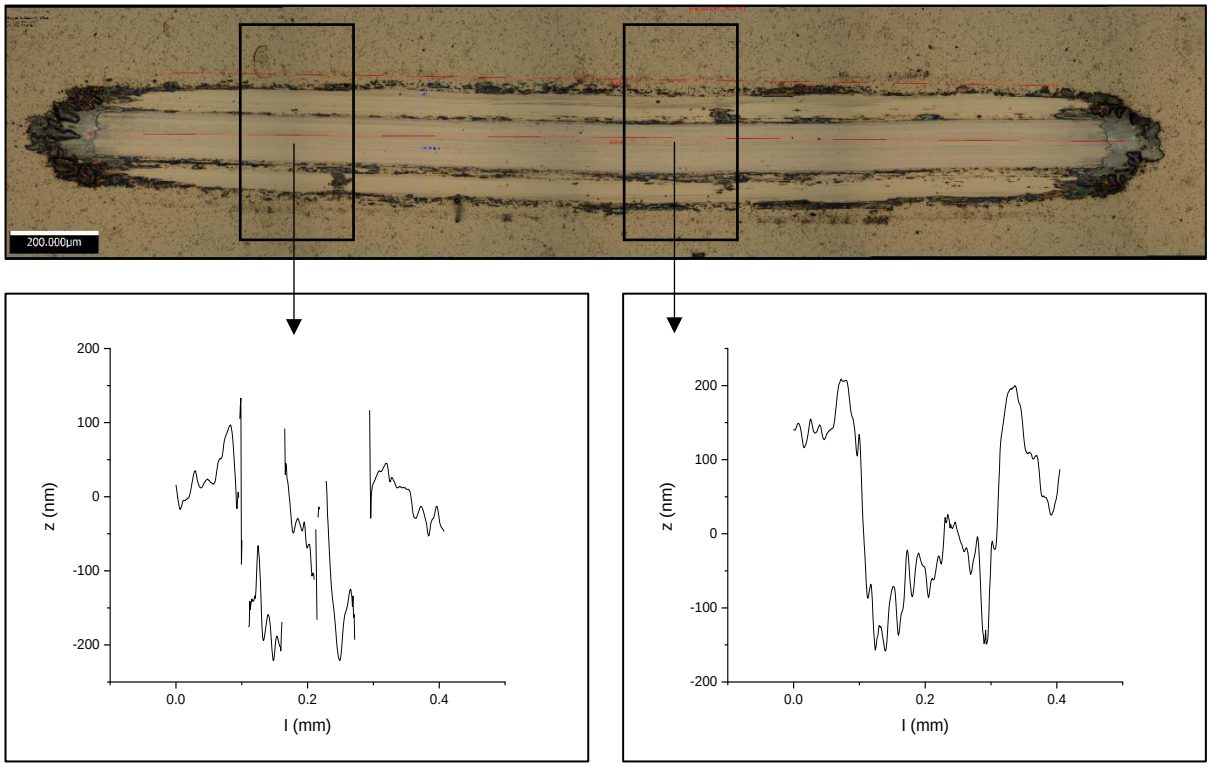

Figure 27. Wear track image of WSC50 with sample depth measurements from 3D optical microscopy from elevated temperature experiments.

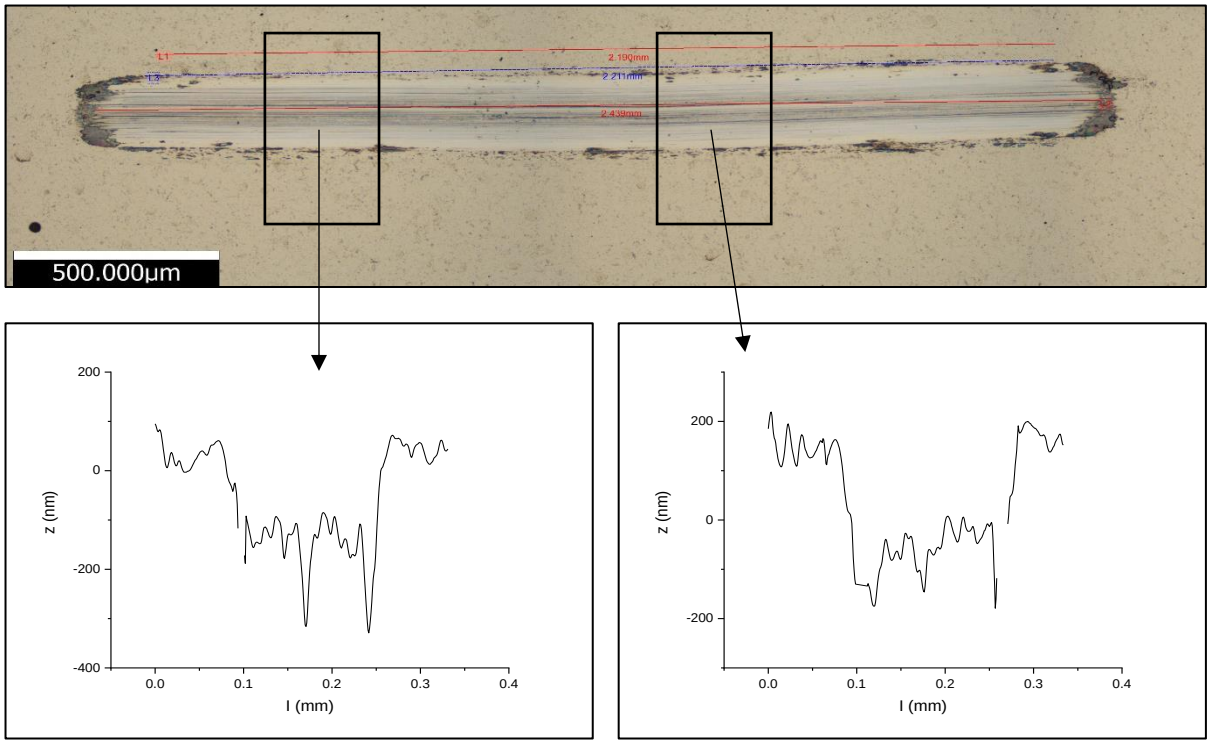

Figure 28. Wear track image of WSC35 with sample depth measurements from 3D optical microscopy from elevated temperature experiments.

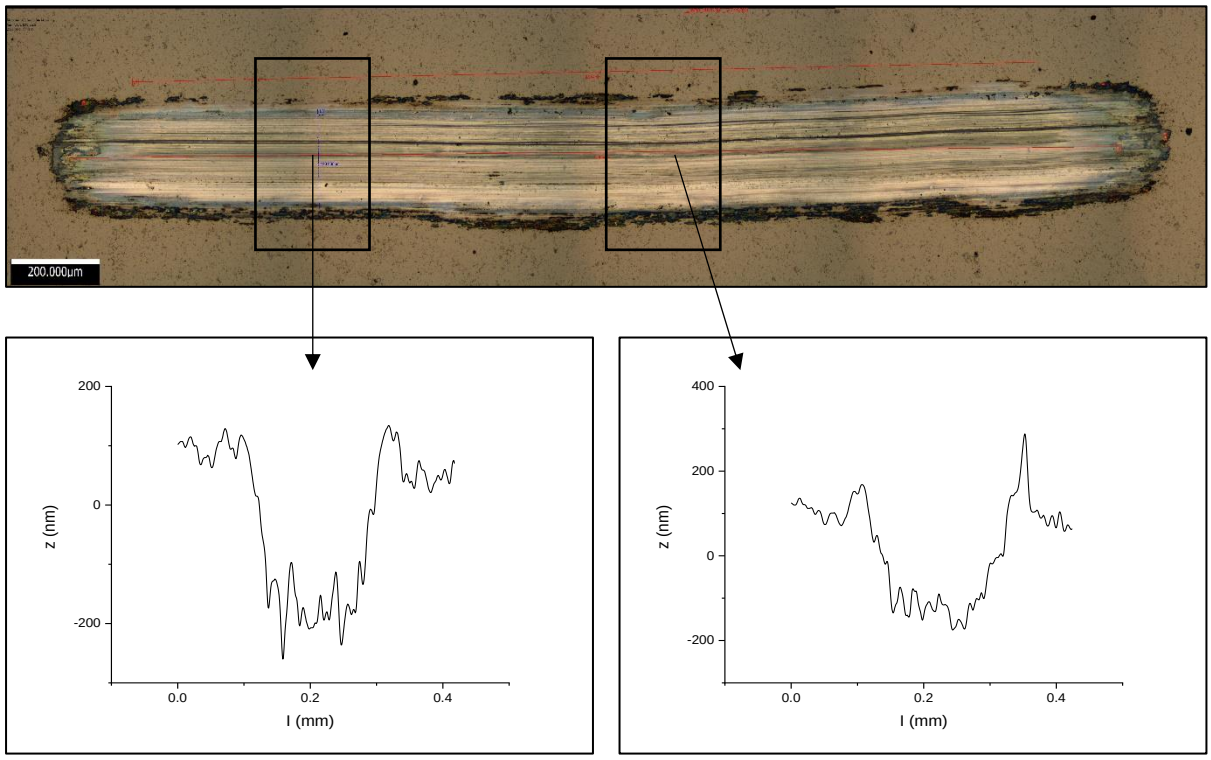

Figure 29. Wear track image of WSCG1 with sample depth measurements from 3D optical microscopy from elevated temperature experiments.

8. Conclusion

Three variants of W-S-C coating were prepared using a DC closed field unbalanced magnetron sputtering system. The three types of coatings are W-S-C with ~50 at.% carbon (WSC50), W-S-C with ~35 at.% carbon (WSC35), and W-S-C with a graded structure (WSCG1). The coating with a graded structure had layers of gradually decreasing carbon content that started with W-S-C at ~50 at.% carbon on the bottom layer and finished with pure WS_2 on the top layer.

WDS analysis confirmed that the reduction of carbon content from ~50 at.% to ~35 at.% was coupled with an increase of sulfur and tungsten contents. X-ray diffractograms of WSC50 and WSC35 show a broad peak which indicated a largely amorphous structure. However, sharp peaks belonging to WS_2 planes are observed in the x-ray diffractogram of WSCG1.

The coatings' micrographs displayed that all coatings manifested a cauliflower-like structure from the top view and showed the absence of prominent columnar structure from the cross-section view. The result of nanoindentation testing confirmed that the lowering of carbon content to ~35 at.% and the graded structure produced coatings with competitive hardness, with only less than 1 GPa difference when compared to W-S-C at ~50 at.% carbon content.

The tribological performance of each coating was tested under ambient condition (room temperature), under a dry N_2 environment, and at an elevated temperature of 200°C. Since the results showed that a low coefficient of friction was accompanied by low specific wear rates for the coating and the ball counterbody, the determination of the best coating for each condition was practical. The coating with ~50 at.% carbon content worked the best under room temperature. The coating with ~35 at.% carbon content performed the best under an elevated temperature. Finally, the coating with the graded structure was superior under a dry N_2 environment.

This work has established modifications on W-S-C coatings that can produce self-adaptive coatings that are suitable for a variety of conditions. The lowering of carbon content to ~35 at.% from ~50 at.% ensured that the coating had a greater amount of available sulfur and tungsten to form lubricous WS_2 crystals upon sliding. The graded structure provided the W-S-C coating with easily shearable top layers for friction reduction and harder bottom layers to carry the load, thus producing an effective solid lubricant coating, especially for sliding in inert environment. This study shows the possibility to adjust the tribological performance of the

coatings depending on the operating conditions, through the usage of specifically designed graded structures.

9. References

[1] H. P. Jost, “Tribology - Origin And Future,” *Wear*, vol. 136, pp. 1–17, 1990.

[2] K. Holmberg and A. Erdemir, “Influence of tribology on global energy consumption, costs and emissions,” *Friction*, vol. 5, no. 3, pp. 263–284, 2017.

[3] Tribology Science Industrial Application Status and Development Strategy, “The investigation on position and function of tribology in industrial energy conservation, consumption and emission reduction (Report of 2 years Chinese Investigation).,” 2008.

[4] H. P. Jost, “Lubrication (Tribology): a report on the present position and industry’s needs. Report to the UK Department of Education and Science.,” 1966.

[5] T. Polcar, A. Nossa, M. Evaristo, and A. Cavaleiro, “Nanocomposite coatings of carbon-based and transition metal dichalcogenides phases: A Review,” *Rev. Adv. Mater. Sci.*, vol. 15, no. 2, pp. 118–126, 2007.

[6] S. Manzeli, D. Ovchinnikov, D. Pasquier, O. Yazyev, and A. Kis, “2D Transition Metal Dichalcogenides,” *Nat. Rev. Mater.*, vol. 2, no. 17033, 2017.

[7] X. Zhou, H. Sun, and X. Bai, “Two-Dimensional Transition Metal Dichalcogenides: Synthesis, Biomedical Applications and Biosafety Evaluation,” *Front. Bioeng. Biotechnol.*, vol. 8, no. 236, 2020.

[8] T. Polcar and A. Cavaleiro, “Review on self-lubricant transition metal dichalcogenide nanocomposite coatings alloyed with carbon,” *Surf. Coat. Technol.*, vol. 206, pp. 686–695, 2011.

[9] M. Evaristo, T. Polcar, and A. Cavaleiro, “Tribological behaviour of C-alloyed transition metal dichalcogenides (TMD) coatings in different environments,” *Int. J. Mech. Mater. Des.*, vol. 4, pp. 137–143, 2008.

[10] K. H. Kannur *et al.*, “Synthesis and structural properties of Mo-S-N sputtered coatings,” *Appl. Surf. Sci.*, vol. 527, 2020.

[11] W. Choi, N. Choudhary, G. H. Han, J. Park, D. Akinwande, and Y. H. Lee, “Recent development of two-dimensional transition metal dichalcogenides and their applications,” *Mater. Today*, vol. 20, no. 3, pp. 116–130, 2017.

[12] B. J. Irving, P. Nicolini, and T. Polcar, “On The Lubricity of Transition Metal Dichalcogenides: an ab initio Study,” *Nanoscale*, vol. 9, no. 17, pp. 5597–5607, 2017.

[13] A. A. Voevodin, J. P. O’Neill, and J. S. Zabinski, “Nanocomposite tribological coatings for aerospace applications,” *Surf. Coat. Technol.*, vol. 116–119, pp. 36–45, 1999.

[14] T. Polcar and A. Cavaleiro, “Self-adaptive low friction coatings based on transition metal dichalcogenides,” *Thin Solid Films*, vol. 519, pp. 4037–4044, 2011.

[15] H. Xiao and S. Liu, “2D Nanomaterials as lubricant additive: A Review,” *Mater. Des.*, vol. 135, pp. 319–332, 2017.

[16] F. P. Bowden and D. Tabor, “Mechanism of Metallic Friction,” *Nature*, vol. 150, pp. 197–199, 1942.

[17] Q. Li, Q. Zhou, L. Shi, Q. Chen, and J. Wang, “Recent advances in oxidation and degradation mechanisms of ultrathin 2D materials under ambient conditions and their passivation strategies,” *J. Mater. Chem. A*, vol. 7, pp. 4291–4312, 2019.

[18] H. S. Khare and D. L. Burris, “The Effects of Environmental Water and Oxygen on the Temperature-Dependent Friction of Sputtered Molybdenum Disulfide,” *Tribol. Lett.*, vol. 52, no. 3, pp. 485–493, 2013.

[19] A. A. Voevodin and J. S. Zabinski, “Supertough wear-resistant coatings with ‘chameleon’ surface adaptation,” *Thin Solid Films*, vol. 370, pp. 223–231, 2000.

[20] T. W. Scharf, A. Rajendran, R. Banerjee, and F. Sequeda, “Growth, structure and friction behavior of titanium doped tungsten disulphide (Ti-WS2) nanocomposite thin films,” *Thin Solid Films*, vol. 517, no. 19, pp. 5666–5675, 2009.

[21] A. Rapuc, K. Simonovic, T. Huminiuc, A. Cavaleiro, and T. Polcar, "Nanotribological Investigation of Sliding Properties of Transition Metal Dichalcogenide Thin Film Coatings," *ACS Appl. Mater. Interfaces*, vol. 12, pp. 54191–54202, 2020.
[22] M. Evaristo, A. Nossa, and A. Cavaleiro, "W–S–C sputtered films: Influence of the carbon alloying method on the mechanical properties," *Surf. Coat. Technol.*, vol. 200, no. 1, pp. 1076–1079, 2005.
[23] A. Nossa and A. Cavaleiro, "Mechanical behaviour of W–S–N and W–S–C sputtered coatings deposited with a Ti interlayer," *Surf. Coat. Technol.*, vol. 163–164, pp. 552–560, 2003.
[24] T. Vuchkov, M. Evaristo, T. B. Yaqub, and A. Cavaleiro, "The effect of substrate location on the composition, microstructure and mechano-tribological properties of W-S-C coatings deposited by magnetron sputtering," *Surf. Coat. Technol.*, vol. 386, 2020.
[25] H. Cao, W. Feng, S. Kumar, R. Petra, J. Hosson, and Y. Pei, "On the S/W stoichiometry and triboperformance of WSxC(H) coatings deposited by magnetron sputtering," *Surf. Coat. Technol.*, vol. 365, pp. 41–51, 2019.
[26] T. B. Yaqub, S. Bruyere, J.-F. Pierson, T. Vuchkov, and A. Cavaleiro, "Insights into the wear track evolution with sliding cycles of carbon-alloyed transition metal dichalcogenide coatings," *Surf. Coat. Technol.*, vol. 403, 2020.
[27] D. M. Mattox, *Handbook of Physical Vapor Deposition (PVD) Processing*, 2nd ed. Elsevier, 2010.
[28] H. Adachi, K. Wasa, I. Kanno, and H. Kotera, *Handbook of sputter deposition technology fundamentals and applications for functional thin films, nano-materials and MEMS*, 2nd ed. Waltham, MA: William Andrew, 2012.
[29] D. Lundin, T. Minea, and J. T. Gudmundsson, *High Power Impulse Magnetron Sputtering: Fundamentals, Technologies, Challenges and Applications*. Elsevier, 2020.
[30] Teer Coatings Ltd, "Closed Field Unbalanced Magnetron Sputter Ion Plating," UK Patent No 2 258 343, 1990
[31] M. E. McConney, "Direct synthesis of ultra-thin large area transition metal dichalcogenides and their heterostructures on stretchable polymer surfaces," *J. Mater. Res.*, vol. 31, no. 7, pp. 967–974, 2016.
[32] T. Vuchkov, T. B. Yaqub, M. Evaristo, and A. Cavaleiro, "Synthesis, microstructural and mechanical properties of self-lubricating Mo-Se-C coatings deposited by closed-field unbalanced magnetron sputtering," *Surf. Coat. Technol.*, vol. 394, 2020.
[33] M. Shamshiri, "Influence of laser structural patterning on the tribological performance of C-alloyed W-S coatings," *Surf. Coat. Technol.*, vol. 394, 2020.
[34] C. Schuh, "Nanoindentation studies of materials," *Mater. Today*, vol. 9, no. 5, pp. 32–40, 2006.
[35] J. Valli, "A review of adhesion test methods for thin hard coatings," *J. Vac. Sci. Technol. A*, vol. 4, no. 6, 1986.
[36] R. Jacobs *et al.*, "A certified reference material for the scratch test," *Surf. Coat. Technol.*, vol. 174–175, pp. 1008–1013, 2003.
[37] N. M. Jennett and S. Owen-Jones, *The Scratch Test: Calibration, Verification and the Use of a Certified Reference Material*. United Kingdom: National Physical Laboratory, 2002.
[38] ASTM International, "ASTM Standard G133-05 Standard Test Method for Linearly Reciprocating Ball-on-Flat Sliding Wear." 2016.
[39] F. Levy and J. Moser, "High-resolution cross-sectional studies and properties of molybdenite coatings," *Surf. Coat. Technol.*, vol. 68–69, pp. 433–438, 1994.

[40] H. Dimigen, H. Hubsch, P. Willich, and K. Reichelt, “Stoichiometry and friction properties of sputtered MoSx layers,” *Thin Solid Films*, vol. 129, no. 1–2, pp. 79–91, 1985.
[41] G. Weise *et al.*, “Preparation, structure and properties of MoSx films,” *Thin Solid Films*, vol. 298, no. 1–2, pp. 98–106, 1997.
[42] J. Sundberg, H. Nyberg, E. Sarhammar, T. Nyberg, S. Jacobson, and U. Jansson, “Influence of composition, structure and testing atmosphere on the tribological performance of W–S–N coatings,” *Surf. Coat. Technol.*, vol. 258, pp. 86–94, 2014.
[43] C. Muratore and A. A. Voevodin, “Control of molybdenum disulfide basal plane orientation during coating growth in pulsed magnetron sputtering discharges,” *Thin Solid Films*, vol. 517, no. 19, 2009.
[44] M. Shamshiri, “Influence of Laser Structural Patterning On The Tribological Performance Of C-Alloy TMD Coatings,” University of Coimbra, 2019.
[45] A. Berkdemir, H. R. Gutierrez, A. Botello-Mendez, N. Perea-Lopez, and A. L. Elias, “Identification of individual and few layers of WS2 using Raman Spectroscopy,” *Sci. Rep.*, vol. 3, 2013.
[46] A. C. Ferrari and J. Robertson, “Interpretation of Raman spectra of disordered and amorphous carbon,” *Phys. Rev. B*, vol. 61, 1999.
[47] A. Nossa, A. Cavaleiro, N. J. M. Carvalho, B. J. Kooi, and J. Th. M. De Hosson, “On the microstructure of tungsten disulfide films alloyed with carbon and nitrogen,” *Thin Solid Films*, vol. 484, no. 1–2, pp. 389–395, 2005.
[48] H. Cao, F. Wen, J. Th. M. De Hosson, and Y. Pei, “Instant WS2 platelets reorientation of self-adaptive WS2/a-C tribocoating,” *Mater. Lett.*, vol. 229, pp. 64–67, 2018.
[49] F. Gustavsson, F. Svahn, U. Bexell, and S. Jacobson, “Nanoparticle based and sputtered WS2 low-friction coatings — Differences and similarities with respect to friction mechanisms and tribofilm formation,” *Surf. Coat. Technol.*, vol. 232, pp. 616–626.
[50] T. W. Scharf and S. V. Prasad, “Solid lubricants: a review,” *J. Mater. Sci.*, vol. 48, pp. 511–531, 2012.